


 Cite this: *RSC Adv.*, 2023, **13**, 47

## Antiviral role of nanomaterials: a material scientist's perspective

 Muhammad Aanish Ali, <sup>a</sup> Nagina Rehman,<sup>b</sup> Tae Joo Park <sup>\*c</sup>  
 and Muhammad Abdul Basit <sup>\*a</sup>

The present world continues to face unprecedented challenges caused by the COVID-19 pandemic. Collaboration between researchers of multiple disciplines is the need of the hour. There is a need to develop antiviral agents capable of inhibiting viruses and tailoring existing antiviral drugs for efficient delivery to prevent a surge in deaths caused by viruses globally. Biocompatible systems have been designed using nanotechnological principles which showed appreciable results against a wide range of viruses. Many nanoparticles can act as antiviral therapeutic agents if synthesized by the correct approach. Moreover, nanoparticles can act as carriers of antiviral drugs while overcoming their inherent drawbacks such as low solubility, poor bioavailability, uncontrolled release, and side effects. This review highlights the potential of nanomaterials in antiviral applications by discussing various studies and their results regarding antiviral potential of nanoparticles while also suggesting future directions to researchers.

 Received 11th October 2022  
 Accepted 9th December 2022

DOI: 10.1039/d2ra06410c

[rsc.li/rsc-advances](https://rsc.li/rsc-advances)

### 1. Introduction

The modern world faces serious challenges due to viral infections and their outbreaks in the form of epidemics and pandemics. Viruses are basically small obligate parasites and

are non-living things residing outside of the host cell. These viruses interact with cells *via* various mechanisms such as receptor–ligand interactions. Among these, respiratory viruses pose a crucial threat to all sorts of demographics. Researchers continue to work on their treatment and suppression by

<sup>a</sup>Department of Materials Science and Engineering, Institute of Space Technology, Islamabad 44000, Pakistan. E-mail: [ab\\_saim@hotmail.com](mailto:ab_saim@hotmail.com); [m.abdulbasit@mail.ist.edu.pk](mailto:m.abdulbasit@mail.ist.edu.pk)

<sup>b</sup>Department of Zoology, Government College University Allama Iqbal Road, Faisalabad 38000, Pakistan

<sup>c</sup>Department of Materials Science and Chemical Engineering, Hanyang University, Ansan 15588, Republic of Korea. E-mail: [tjp@hanyang.ac.kr](mailto:tjp@hanyang.ac.kr)



Engr Muhammad Aanish received his bachelor's degree in Materials Science and Engineering from Institute of Space Technology (IST), Islamabad, Pakistan in September 2022. He is an active researcher in the fields of development of Nanomaterials for various engineering applications such as photovoltaics and biotechnological treatment of waste water. He is currently a member of

research group “Nanomaterials for Advanced Energy Applications” (NAEA) headed by Dr Basit at IST. He has participated in several review/research papers during his academic career so far. His key ambition is to conduct extensive and valuable research that could provide a good value to research community.



Dr Nagina Rehman graduated in Zoology from Bahauddin Zakariya University Multan, Pakistan in 2009. Then she joined University of Agriculture Faisalabad to accomplish her MPhil Zoology in 2013 with research specialization of biodiversity. Having PhD from Government College University Faisalabad Pakistan (2020), Dr Nagina chose a multidisciplinary research career in

Nanotechnology for Zoological Species. She is currently working as Assistant Professor at Riphah University, Faisalabad (Campus) and motivated to investigate and research the toxicological effect/control of nanomaterials in human beings.



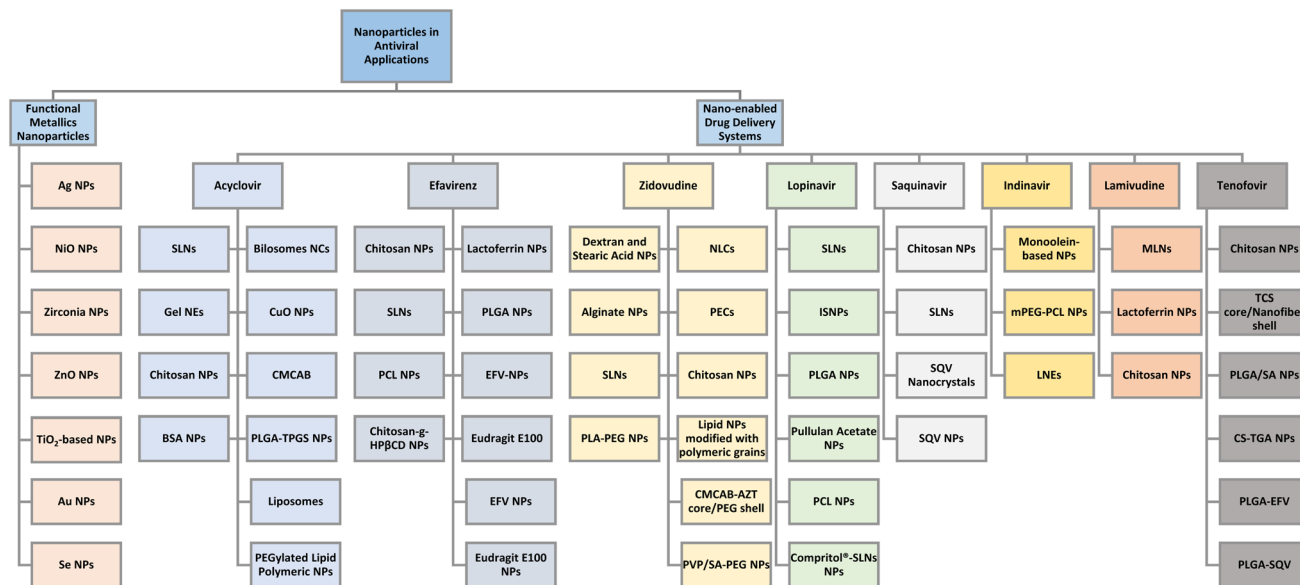


Fig. 1 An overview of applications of nanoparticles and their combinations with a variety of antiviral drugs.

utilizing nano-based options such as functional metallic nanoparticles (NPs) and nano-enabled drug delivery systems. The drug delivery systems must be capable of dealing with inherent features of viral infections like their replication dynamics, level of drug resistance, and complex lifecycle stages. Frequent drug use causes enhancement of drug resistance against viruses and has now become a crucial health issue globally for nearly all sorts of drugs that are known to be effective against one or more specific viruses. The past two decades have witnessed the emergence of old viral infections and introduction of new types of viruses such as severe acute respiratory syndrome (SARS-CoV-2) which is a form of coronavirus.<sup>1-4</sup> The human body can contract these viruses *via* various routes such as ear, nose, mouth, and skin.<sup>5</sup> Once a virus

is contracted, it is difficult for the human body to develop an immune response against it. Due to larger categories of viruses than the number of treatment options available, there are still many infections for which there is either no effective treatment or treatment has not proved to be fully effective.<sup>6</sup>

Besides posing threat to human health and life, the viral outbreaks have affected human life in several ways ranging from disruption of daily life activities, economic collapse of societies, shortages of food and medical supplies, and mass-scale deaths.<sup>7,8</sup> A recent example is of COVID-19 pandemic in which the world witnessed the peak of these problems till the time when an adequate number of vaccine doses were administered globally to most of the population and the trends showed a decline in emergence of new cases and decrease in



*Dr Tae Joo Park is currently serving as Professor of Materials Science & Chemical Engineering at Hanyang University (HYU) Ansan, Republic of Korea. Dr Park has PhD from Seoul National University, Korea and research experience from University of Texas Dallas, USA. He established Nanodevice Engineering Laboratory at HYU and conducted many funded research projects in parallel to*

*the research supervision of many local/international students in the domain of energyharvesting/storage/nanoelectronic/neuromorphic devices, film/particle ALD and 2D-electron gas. Owing to expertise in research and innovation, Dr Park has won many awards and honors from various firms including Samsung (2019) and Merck (2021) etc.*



*Dr Muhammad Abdul Basit is serving as Associate Professor at Department of Materials Science & Engineering at IST Pakistan, where he established: "Nanomaterials for Advanced Energy Applications" research group too. After having graduation from UET Lahore, Dr Basit joined BZU Multan as Lecturer and received MS-leading PhD scholarship by Higher Education Commission of Pakistan (2011-*

*16) for his PhD from NEL-HYU, South Korea. In addition to post-doctoral research at HYU, he won intellectual capability awards from various agencies such as PCK (2012), DAAD-Germany (2017) etc. He holds reputable record for scientific publications/keynotes/book chapters as well as research in arts (Urdu Poetry/Iqbal).*



deaths due to increased immunity among people, thanks to these vaccines.

Research has previously shown that nanomaterials possess great potential in antiviral applications.<sup>9</sup> Materials scientists and chemists have conducted extensive research to explore and synthesize newer, efficient nanomaterials which can successfully inhibit and treat a wide range of viruses. Different functional NPs and nanostructures have shown antiviral activities against a broad spectrum of viruses, each having its mechanism and viricidal activity. Every system comes with its limitations and benefits and hence it is important to employ the most suitable candidate for treatment of specific viruses.<sup>10</sup> Fig. 1 presents an outlook on the use of nanoparticles and nano-based drug delivery systems which have proved to be effective against many viruses.

Before the advent and advance of nanotechnology, antiviral drugs were extensively used for treatment of viruses. The efficiency of these drugs was limited due to their inherent low bioavailability, shorter half-life, cytotoxicity, uncontrolled release as well as serious side effects that limited their use.<sup>11,12</sup> Material scientists have developed nanoparticles that were capable of acting as delivery vehicles for these drugs, releasing a controlled amount of drug to the targeted site for the required amount of time. They showed appreciable entrapment of drug while increasing the efficacy and enhancing the viricidal effects. The key property of nano-enabled delivery systems is that due to their extremely smaller size and high surface areas, they facilitate better digestion, absorption, and penetration of drugs.<sup>13,14</sup> In this review, we have discussed well-known functional NPs which exhibit antiviral action, their synthesis, properties, and mechanism along with exhaustive and informative discussion of existing nano-enabled drug delivery systems which are known to have overcome the limitations of antiviral drugs such as low biocompatibility, cytotoxicity, hemocompatibility and difficulty in administration to patients, among various other issues associated with them which we have covered in this review.

## 2. Metal-based nanoparticles as effective antivirals

### 2.1 Ag-based NPs

Silver nanoparticles (AgNPs) have shown great potential in biomedical applications such as anti-bacterial and anti-cancer. However, there is only a handful of research on antiviral activity of Ag-based NPs. Results from recent studies show that AgNPs are quite effective against a wide range of viruses such as respiratory syncytial virus (RSV), enterovirus 71, herpesvirus (HSV-1 and HSV-2), poliovirus (PV), dengue virus (DENV), influenza (H1N1, H3N2), hepatitis (HSV-1, HAV-10, and CoxB4) and coronaviruses (porcine epidemic diarrhea virus (PEDV) and feline coronavirus (FCoV)).<sup>15</sup>

Morris *et al.* reported the first *in vivo* study to examine the antiviral nature of AgNPs against RSV infections. A significant decrease in pro-inflammatory cytokines and chemokines was recorded in the infected mice's lungs. AgNPs were able to

effectively block the entry of RSV to host cells by binding to the surface of glycoproteins and inhibiting the spread of RSV. While the development of vaccines for RSV infections remains a challenge, employing AgNPs can be a novel strategy to treat RSV-infected patients.<sup>16</sup> While small interfering RNA (siRNA) holds promise in antiviral activity against EV71, its major limitation is its inability to cross cell membranes. The study prepared surface-decorated AgNPs using polyethyleneimine (PEI) and siRNA and monitored for their antiviral activity. The accumulation of reactive oxygen species (ROS) was effectively inhibited, and EV71 was not able to infect the host cells.<sup>17</sup> The potential of AgNPs against PV was monitored *in vitro*, as the electrochemically synthesized AgNPs played a key role in the disinfection of PV, a non-enveloped virus.<sup>18</sup>

The use of AgNPs in antiviral applications is generally limited since many AgNPs are synthesized in a liquid atmosphere, a technique not easily applicable. Recent studies have suggested numerous solutions to address this limitation. Szymańska *et al.* reported preparation of mucoadhesive hydrogel based on tannic acid (TA)-modified AgNPs (TA-AgNPs) as an effective route for treatment of HSV-1 and HSV-2.<sup>19</sup> For enhancing the antiviral action, the NPs were encapsulated by a hydrogel called Carbopol 974P for effective delivery to the targeted site (*ex vivo* vaginal mucosa). The gelation (100% crosslinking) was facilitated by an initiator, thereby providing closer contact between drug carrier and the mucosal tissue. The size of nanoparticles was found to be between 13 and 54 nm as estimated from the micrographs of transmission electron microscope (TEM) (Fig. 2(a) and (b)). The antiviral efficacy of NP-based hydrogel was evaluated *in vitro*. To ensure that components of hydrogel do not affect the infectivity of HSV-1 and 2, placebo hydrogel and TA-AgNPs were simultaneously applied. The scheme of virus inhibition assay is illustrated in Fig. 2c(A). Both types of HSVs were considerably inhibited after a 24 h incubation period, which indicates the potential of prepared formulation against HSV infections. However, the inhibition was roughly 20% more for HSV-2 (Fig. 2c(B)). The results shown in Fig. 2c(C) and (D) indicate that inhibition of HSV-1 and 2 is greater in cells that were exposed to hydrogels as compared to the control cells, with more inhibition in case of HSV-2. It is pertinent to mention that inhibition rate of HSV-1 infection was dependent on the concentration of the NPs in hydrogel while concentration played no role in inactivation of HSV-2. Possible mechanisms of virus suppression may be due to NP interacting with HSV envelope and blockage of virus interaction with cells due to layer of hydrogel around them. The study further explored the mode of antiviral activity of prepared formulation by employing assays of virus attachment and penetration. The variables of both assays are shown in Fig. 2d(A). After 24 h post-infection, it was observed that around 85–90% inhibition for HSV-1 attachment to the cell surface with a considerable decrease in plaque numbers (greater than 60%) was recorded for HSV-2 (Fig. 2d(B)). This time the percentage of HSV-1 inhibition after treatment with H2/NP25 (Fig. 2d(B)) was found to be greater than the inhibition of HSV-2. The penetration assay showed that HSV-2 entry to HaCaT cells was suppressed by exposure to both hydrogels. Interestingly, both



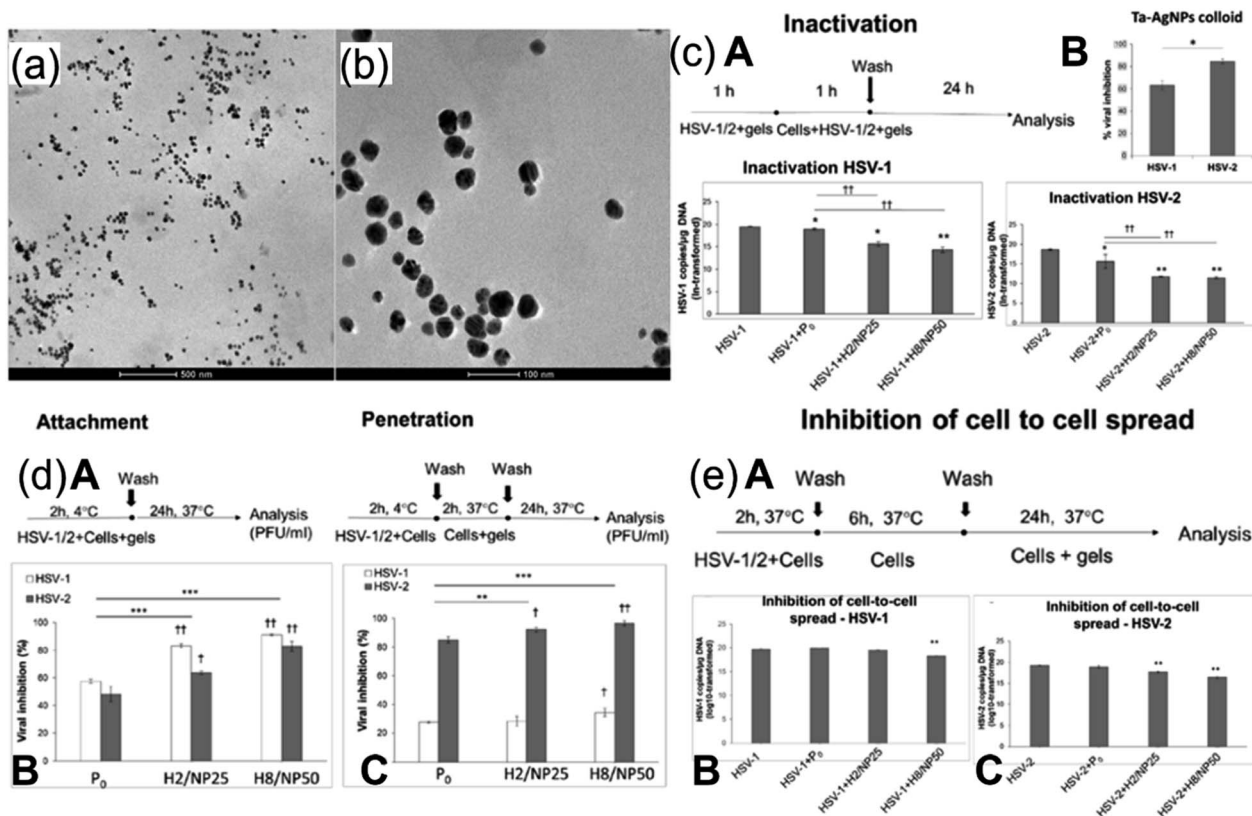


Fig. 2 TEM images of H2/NP25 hydrogel containing 25 parts per million (ppm) TA-AgNPs. (a) Shows a scale bar of 500 nm; (b) shows a scale bar of 100 nm. (c) (A) HSV inhibition assay; (B) inhibition of HSV-1 and HSV-2 in HaCaT cells; (C) DNA titers of HSV-1; (D) of HSV-2. (d) (A) HSV attachment and penetration scheme; (B) HSV-1 and HSV-2 attachment and (C) penetration. (e) (A) Cell-to-cell inhibition assay scheme; (B) DNA titers of HSV-1 and (C) HSV-2 (reprinted with permission from ref. 19 Copyrights 2018 MDPI).

formulations of hydrogel showed lower inactivation for HSV-1 in contrast to attachment assay. NPs inside the cell could have played a vital role in inhibition. Hence cell-to-cell spread assays were conducted (Fig. 2e). It can be seen that the inhibitory effect of both hydrogels on the cells infected with HSV-2 is significantly greater than that of the control and placebo (Fig. 2e(C)). In contrast, the cell-to-cell spread was inhibited for HSV-1 infected cells only by the hydrogel with 50 ppm TA-AgNPs (Fig. 2e(D)). The Carbopol 974P provided two distinct properties; transporting antiviral (TA-AgNPs) to targeted site and inherent antiviral activity. Therefore, a synergistic effect of both hydrogel and NPs played a key role in suppression of HSV infection. The authors, however, suggested the need for future *in vivo* studies for further exploration and innovation of this novel route (readers are suggested to consult the cited literature for information about the specific composition of the H2/NP25 Hydrogel formulation).

Another study reported two algae, *Oscillatoria* sp. and *Spirulina platensis*, mediated by green Ag<sub>2</sub>O/AgO-NPs and Au-NPs, respectively, and evaluated their effect on HSV-1 infection.<sup>20</sup> The spherical-shaped Ag<sub>2</sub>O/AgO-NPs with smaller size (nm) than non-spherical AuNPs showed a greater reduction rate of HSV-1. The results indicate the potential of bio-synthesized NPs as suppressing agents for HSV-1 infection. Remarkable antiviral activity of green synthesized AgNPs of two plant extracts, *L.*

*coccineus* and *M. lutea*, was shown against HSV-1, HAV-10, and CoxB4 virus.<sup>21</sup>

Sreekanth *et al.* reported virucidal effects of AgNPs, 5–15 nm in size, against influenza A virus with an easy, smooth, and convenient approach used for synthesis of AgNPs *i.e.*, ultrasonication method. Green synthesized AgNPs were studied for *in vitro* cytotoxic and antiviral activities and showed to possess good antiviral action against H1N1 variant of Influenza A virus.<sup>22</sup> Another study reported AgNPs (not green synthesized) as potential antiviral agents against H1N1.<sup>23</sup> The potential of AgNPs was shown against H3N2 variant of Influenza virus with the help of *in vitro* and *in vivo* studies.<sup>24</sup> For *in vivo* studies, the survival of mice was enhanced while *in vitro* studies showed that AgNPs were able to protect cells by inhibiting viral infections. The mechanism of antiviral action appeared to be the destruction of virus morphology by AgNPs.

## 2.2 NiO nanostructures (NONS)

The leading cause of the infection in cucumber crops is cucumber mosaic virus (CMV), resulting in a significant reduction in crop yield globally, especially in Egypt. Viral diseases are not usually countered by chemical pesticides, one of the reasons being their ineffectiveness resulting from repeated use.<sup>25</sup> Several studies have related the growth of plants





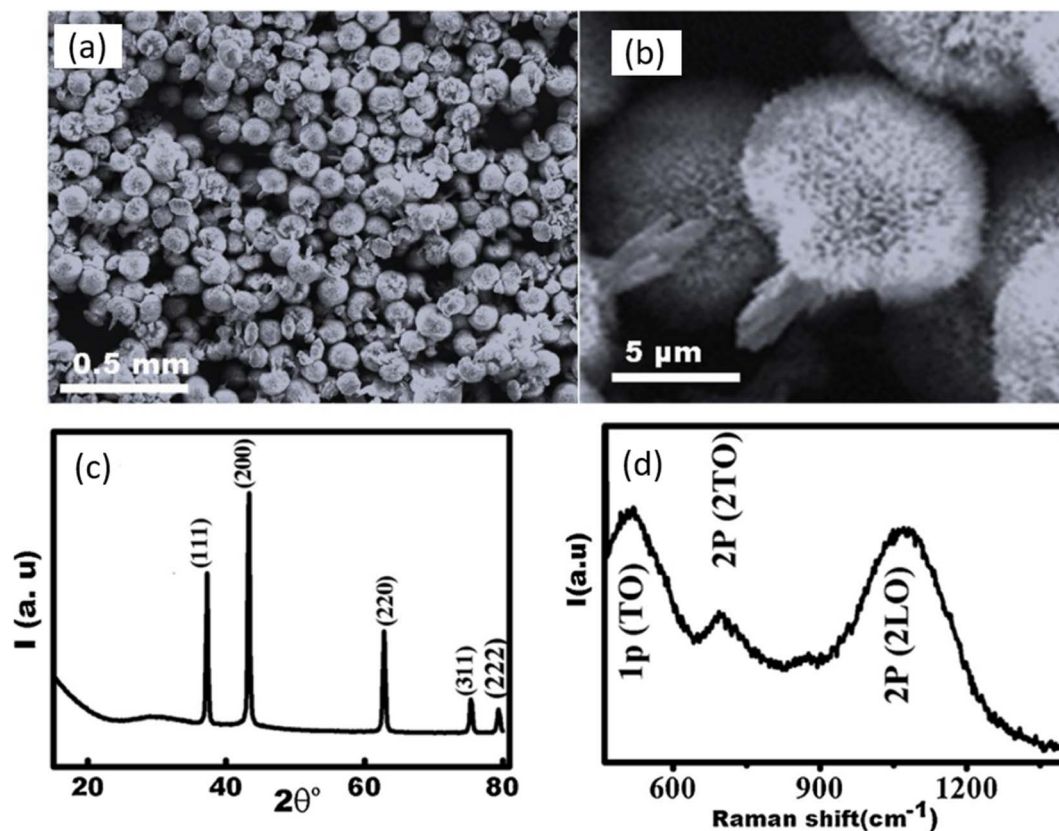


Fig. 3 (a) FESEM micrograph of NONS. (b) FESEM micrograph showing uniform formation of head and trunk. (c) XRD pattern of NONS. (d) Raman spectroscopy results of NONS (reprinted with permission from ref. 26 Copyrights 2019 Elsevier).

with the amount of nickel (Ni) present. The need evolved to investigate the effect of Ni-based nanostructures against CMV.<sup>26</sup> NiO was fabricated *via* one-pot hydrothermal synthesis and the efficacy of NONS against CMV in cucumber plants was evaluated against reduction in disease severity, assessed *via* immunosorbent assay. NONS particles of about 15–20 nm in size with greater exposed surface area were administered *via* foliar spray or soil drench to infected plants. The nanostructures were characterized by FESEM, X-ray diffraction (XRD), and Raman spectroscopy, and results are shown in Fig. 3. FE-SEM images in Fig. 3a and b show stable morphological nanostructures of NiO. Semi-spherical head ends are composed of nanotubes aligned normally within body of head. The distribution of these nanotubes across the surface of head indicates that average size of tube is in between 15 and 20 nm. Moreover, thick distribution of nanotubes resembles tubular vessels resulting from carefully designed NONS. WA-XRD was employed to determine the crystal structure of NONS. Crystal planes are indicated at well-resolved and sharp diffraction peaks of NiO and indicated accordingly in Fig. 3c. Raman spectroscopy revealed the presence of pristine NiO as appeared peaks result from presence of two TO modes and two LO modes as indicated in Fig. 3d. *In vivo* study concluded that plants treated with NONS showed visible reduction in CMV compared to non-treated counterparts, showing potential for NONS to be used as antiviral agent against CMV.

### 2.3 Zirconia NPs

Zirconia NPs have shown promise in treatment of cancer in previous studies, but their antiviral activity was not reported previously. Huo and collaborators studied the antiviral effect of ZrO<sub>2</sub> NPs on H5N1 variant of influenza A virus.<sup>27</sup> The mice infected with H5N1 virus were treated with ZrO<sub>2</sub> NPs of about 200 nm in size and administered intraperitoneally. The *in vivo* study concluded that survival chances of mice were increased by about 85.7%, as the ZrO<sub>2</sub> NPs promoted the release of cytokines in mice. Thus, this novel strategy needs further exploration for future innovations.

### 2.4 ZnO NPs

The antiviral drugs currently employed for the treatment of influenza viruses are becoming insignificant as they cause adverse side effects with drug-resistant strains.<sup>28</sup> There is an urgent need to develop better and more efficient anti-influenza agents. A few advantages of using nanoparticles for the treatment of viral infections are that their synthesis is cheaper, they possess good antiviral efficacy, and can be tailored to improve properties *via* coating. ZnO-NPs have previously shown substantial antimicrobial and antibacterial activities.<sup>29</sup> However, a handful of research has been done to evaluate the antiviral efficacy of ZnO-NPs. Ghaffari *et al.* were the first to examine the antiviral efficacy of ZnO-NPs and PEGylated ZnO-



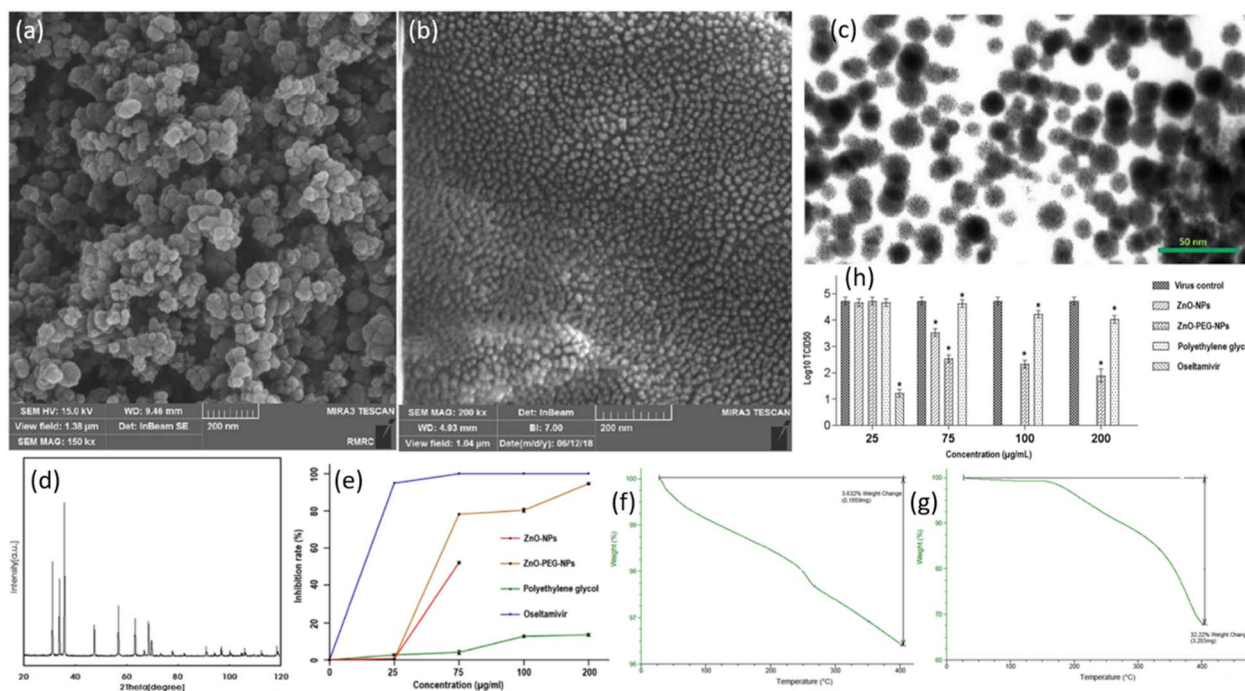


Fig. 4 (a) FESEM micrograph of ZnO-NPs. (b) FESEM micrograph of ZnO-PEG-NPs. (c) TEM micrograph of ZnO-PEG-NPs. (d) Powder XRD results for ZnO-NPs. (e) Real-time PCR assay results for inhibition rates of four compounds against H1N1 influenza. (f) TGA results of ZnO-NPs. (g) TGA of ZnO-PEG-NPs. (h) Post-exposure antiviral activity of different compounds against H1N1 influenza virus assessed via TCID50 assay (reprinted with permission from ref. 30 Copyrights 2019 BioMed Central).

NPs *in vitro*.<sup>30</sup> The size of NPs was reduced to a large extent as a result of massive ball milling. Scanning electron microscopy (SEM) confirmed the sizes of ZnO-NPs to be 20–50 nm and ZnO-PEG-NPs to be 16–20 nm (Fig. 4a). The SEM images show NPs to be of spherical morphology with uniform size distribution. The surface coating of ZnO-NPs was confirmed *via* TEM micrographs in Fig. 4b. The presence of ZnO-NPs was confirmed by XRD power diffraction pattern. When compared to the standard powder diffraction file (PDF), the peaks and their respective intensities of ZnO exhibit a similar pattern as depicted in Fig. 4c. Thermogravimetric analysis (TGA) was employed for weight loss measurements (Fig. 4f and g). It can be seen that at a temperature of 400 °C, there is a significant decrease in weight (%) in the case of ZnO-PEG-NPs (Fig. 4g) while the weight loss is very small at the same temperature for ZnO (Fig. 4f). This gives a reasonable explanation for coating of PEG which resulted in greater weight loss. The key finding of the study was that the NPs cause antiviral action only after the virus has infected the cells. There was considerable inhibition when H1N1 virus was exposed after infection to ZnO-PEG-NPs as there was a significant reduction in virus titers in contrast to the virus control, as shown at concentrations of 75, 100, 200  $\mu\text{g mL}^{-1}$ . The maximum concentration of ZnO-NPs alone could only result in 1.2 log<sub>10</sub> TCID<sub>50</sub> reduction which is much lower than reductions caused due to PEGylated ZnO-NPs. At its maximum non-toxic concentration, PEG alone could reduce by 0.7 log<sub>10</sub> TCID<sub>50</sub>, which is even lower than ZnO-NPs. These results are schematically depicted in Fig. 4h. It was observed in

quantitative real-time PCR tests that significant inhibition resulted by ZnO-PEG-NPs at concentrations of 75, 100, 200  $\mu\text{g mL}^{-1}$ , which are much superior to ZnO-NPs inhibition rates at respective concentrations. However, it is quite interesting to note that oseltamivir was able to fully inhibit influenza at a concentration of 75  $\mu\text{g mL}^{-1}$ . These results are summarized in Fig. 4e. While the precise antiviral mechanism of virus inhibition largely remained unexplored, PEGylating the surface of ZnO-NPs resulted in increased antiviral activity and can be employed as a novel strategy for improving the antiviral efficacy. Hence ZnO-PEG-NPs can be an effective antiviral agent against influenza viruses.

## 2.5 TiO<sub>2</sub>-based NPs

Broad bean stain virus (BBSV) infects seeds of many food crops. Fab bean crop is significant globally, especially in Egypt. They are quite sensitive to viral diseases like BBSV.<sup>31</sup> Recent studies have proposed nanotechnology as a novel method to control pathogens in plants.<sup>32</sup> The excellent property profile offered by TiO<sub>2</sub> allows it to be used in a variety of applications, including antiviral. However, the efficacy of TiO<sub>2</sub> is negatively affected by several factors such as its inherent crystallinity, unfavorable surface-to-size area ratio, and its surface morphology.<sup>33</sup> The material scientists have focused on developing new modes of synthesis of TiO<sub>2</sub> that induce functionalities that can prove effective in the treatment of plant-related diseases. The mechanism of antiviral action against plant viruses can be different and varies from material to material. For instance, it can



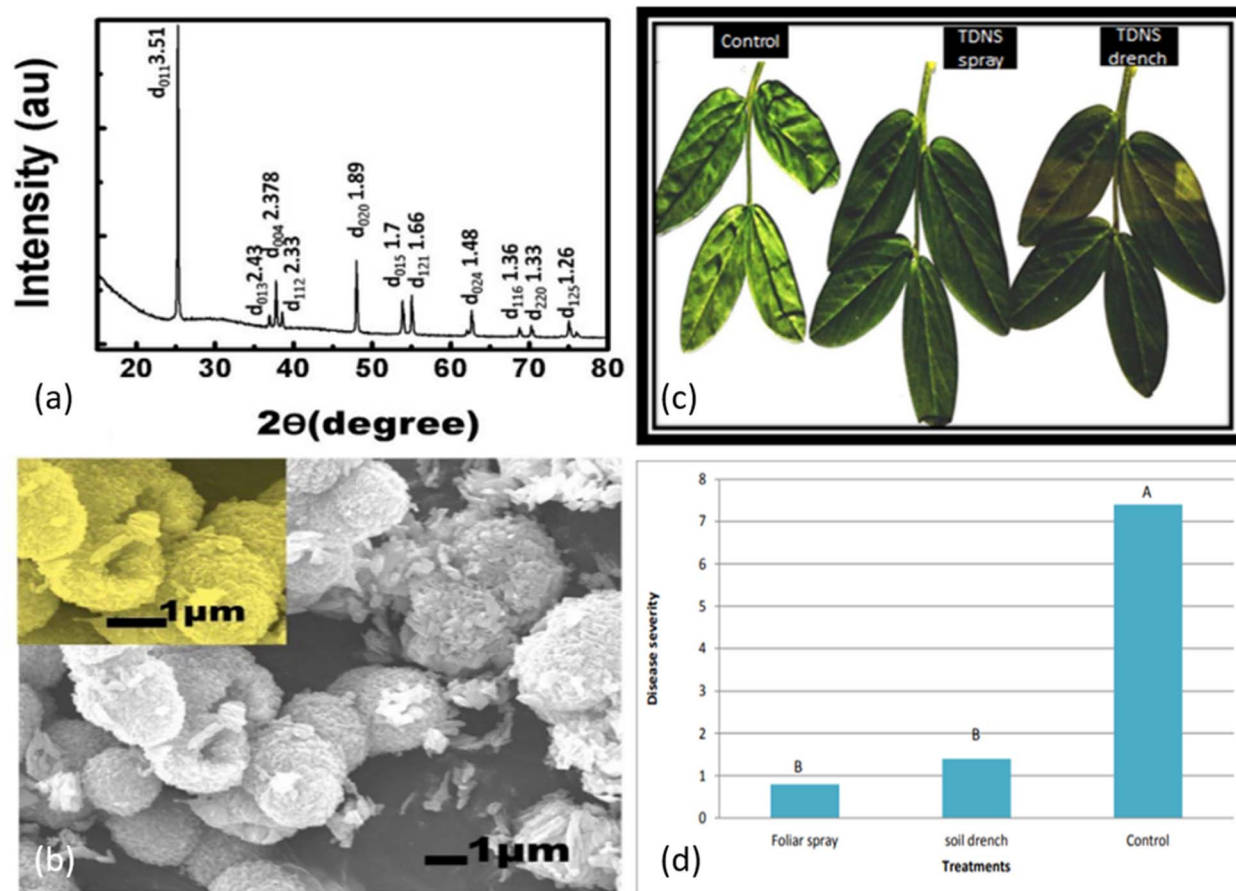


Fig. 5 (a) Wide-angle (WA) XRD pattern of TDNS. (b) FESEM image of TDNS. (c) Symptoms of BBSV caused in un-treated faba plants (control), treated with TDNS via foliar spray and soil drench after 2 weeks. (d) Degree of disease severity in treated plants and un-treated plants (Different letters above columns indicate significant differences by the Steel–Dwass test for faba bean ( $P < 0.05$ )) (reprinted with permission from ref. 35 Copyrights 2018 Society of Chemical Industry).

include the direct effects of NPs against the virus which can result in death of virus or may also cause the defensive system of plants to become stronger and hence increase its inherent immunity to deal with virus.<sup>34</sup> One such study was done by Elsharkaway *et al.*, who fabricated  $\text{TiO}_2$  nanostructures (TDNS) and examined its antiviral efficacy against BBSV.<sup>35</sup> The approach used for synthesis was similar to that reported by Goma *et al.*<sup>36</sup> *i.e.*, direct mild hydrothermal synthesis, with slight changes. To determine the crystal structure of the synthesized NPs, wide-angle X-ray diffraction (WA-XRD) was utilized which shows a similar pattern as that for standard  $\text{TiO}_2$  as seen in Fig. 5a. FE-SEM micrographs confirm the successful synthesis of  $\text{TiO}_2$  structures as surfaces can be seen to be smooth from inside and rough from outside with a small thickness of walls (Fig. 5b). The further morphological examination also shows that size distribution was in the range of 3–5  $\mu\text{m}$  for diameter, while 3–4  $\mu\text{m}$  for length and width. Combining of a large number of  $\text{TiO}_2$  nano-sheets can form a hollow shape as hydrogen from oleic acid bond to  $\text{TiO}_2$  surface.<sup>37</sup> This can result in favorable exposed surface area for interaction between virus and TDNS with greater antiviral activity. Experimental results after a 14 days treatment are

shown in Fig. 5c. The control leaves can be seen to be smaller and deformed while the leaves treated with TDNS exhibited great reduction in symptoms of BBSV. Outstanding reduction in disease severity of faba bean plants due to TDNS can be seen in Fig. 5d. Foliar spray method appeared to be more effective in decreasing the disease severity than soil drench technique. (In foliar spray, fertilizers (in our case  $\text{TiO}_2$  nanostructures or TDNS) are sprayed on the plant leaves rather than pouring them in the soil). In contrast, soil drench technique involves pouring the chemicals mixed with water directly onto the soil). Moreover, concentration of BBSV in plants treated via foliar spray method is also lower than in soil drench. Plants treated with both approaches showed no significant difference in gene expression which was, however, much greater than control. Thus, due to TDNS inducing systematic resistance, there was a significant decrease in disease severity. Structural features of TDNS such as particle size and suitable shape were the governing factors for its good overall efficacy against BBSV. This study is only one of its kind which evaluated and suggested an eco-friendly approach to treating plants against BBSV.

Nakano *et al.* proposed use of TD thin film for photocatalytic inactivation of H1N1 Influenza. This can be attributed to the





strong oxidation effect produced when  $\text{TiO}_2$  is exposed to UV light.<sup>38</sup> The study demonstrated that  $\text{TiO}_2$  substantially increases the disinfection rates of H1N1 by a strong oxidation effect which degrades viral proteins. A slight amendment in the ISO method was made for evaluating the anti-bacterial effects of TD which can prove beneficial for enhancing the antiviral activity. There are a few studies that relate the antiviral mechanism of action of  $\text{TiO}_2$  to the best of our knowledge.

## 2.6 GO-Ag NPs

Nanomaterials are of key importance in treatment of viral infections. In this regard, AgNPs have shown good potential in antiviral actions against a variety of viruses, as discussed before in this review. Chen *et al.* reported that there have been no studies on the antiviral efficacy of nanomaterials against non-

enveloped viruses.<sup>39</sup> Their study evaluated the antiviral activity of GO sheets and GO-AgNPs against both enveloped and non-enveloped viruses. The enveloped virus chosen was Feline Coronavirus (FCoV) while the non-enveloped virus was Infectious Bursal Disease Virus (IBDV). The particle size distribution (PSD) of Ag NPs was between 5–25 nm while thickness of each GO layer was 0.355 nm and there were 2 to 5 layers in total. The virus inhibition assay reported a significant reduction of FCoV (25%) and IBDV (23%) by GO-Ag NPs than GO sheets whose inhibition was restricted to merely 16%. The virus inhibition mechanism of GO-Ag NPs is illustrated schematically in Fig. 6.

## 2.7 Gold nanoparticles (AuNPs)

The exceptional property profile package offered by AuNPs such as exquisite quantum size effect, surface effect, and

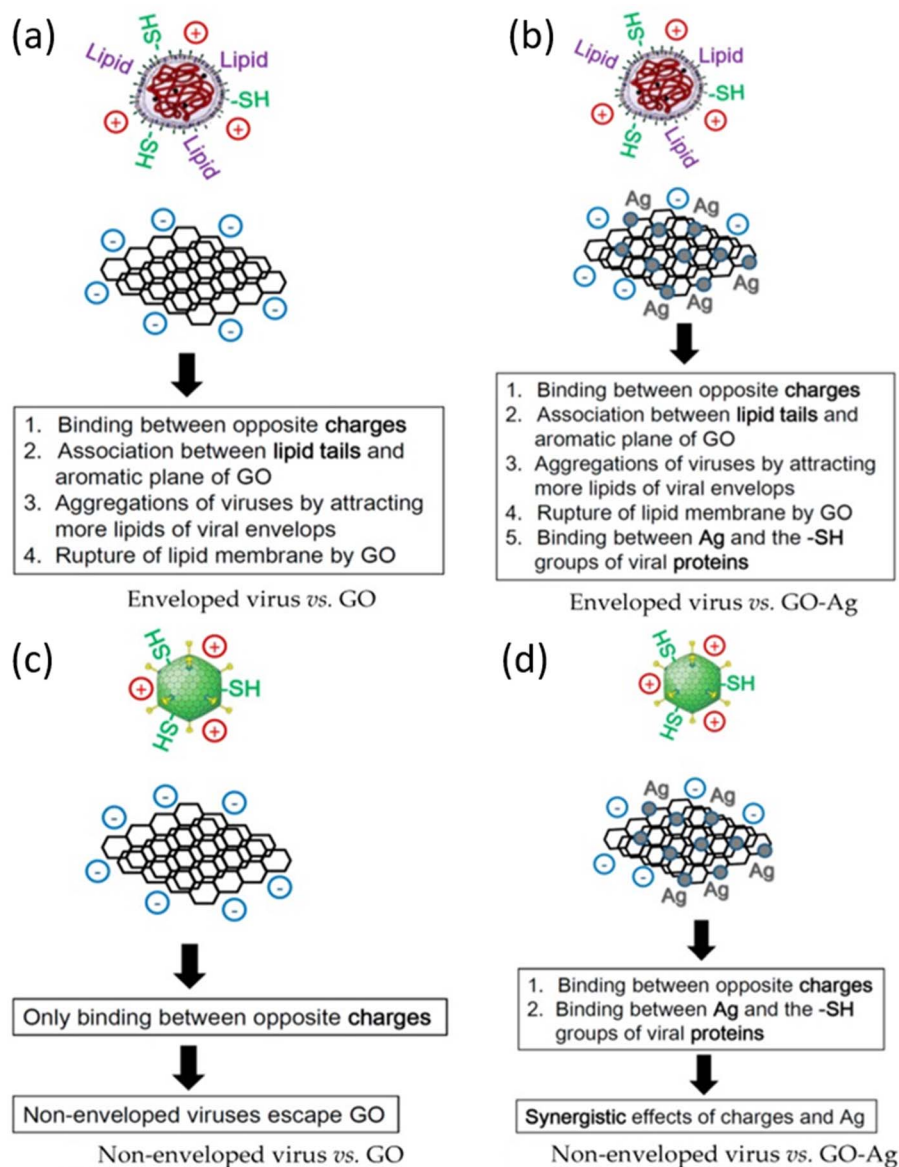


Fig. 6 Schematic illustration of antiviral mechanism of (a) GO; (b) GO-Ag against enveloped viruses; (c) GO and (d) GO-Ag against non-enveloped viruses (reprinted with permission from ref. 39 Copyrights 2016 MDPI).





macroscopic quantum tunneling effect make them useful in nanomedical applications. Several studies have evaluated antiviral efficacy of AuNPs against a variety of viral infections. For example, Asim and his coworkers synthesized AuNPs of  $7.86 \pm 3.3$  nm in size by sonication of gallic acid in a bath Sonicator and examined their antiviral mechanism of action.<sup>40</sup> They reported that AuNPs prevent the attachment and penetration of HSV. The amount of virus inhibited is dependent on the time of exposure of AuNPs and hence the method employed uses highly monodispersed AuNPs. Their bio-friendly nature makes them

a strong candidate for prevention of HSV. Another study reported by Gianvincenzo *et al.* evaluated AuNPs antiviral efficacy against HIV.<sup>41</sup> Two compounds used Au clusters of about 1.7 nm and 2.6 nm, respectively, which accommodated about 140 sulfated ligands and were enough to perform anti-HIV action. The *in vitro* study revealed that AuNPs do this by binding to glycoprotein (gp120). AuNPs can be coated with sulfate-ended ligands which in turn bind the HIV, causing its inhibition. This result opens doors of opportunities to tailor those surface ligands for development of more anti-HIV systems. The

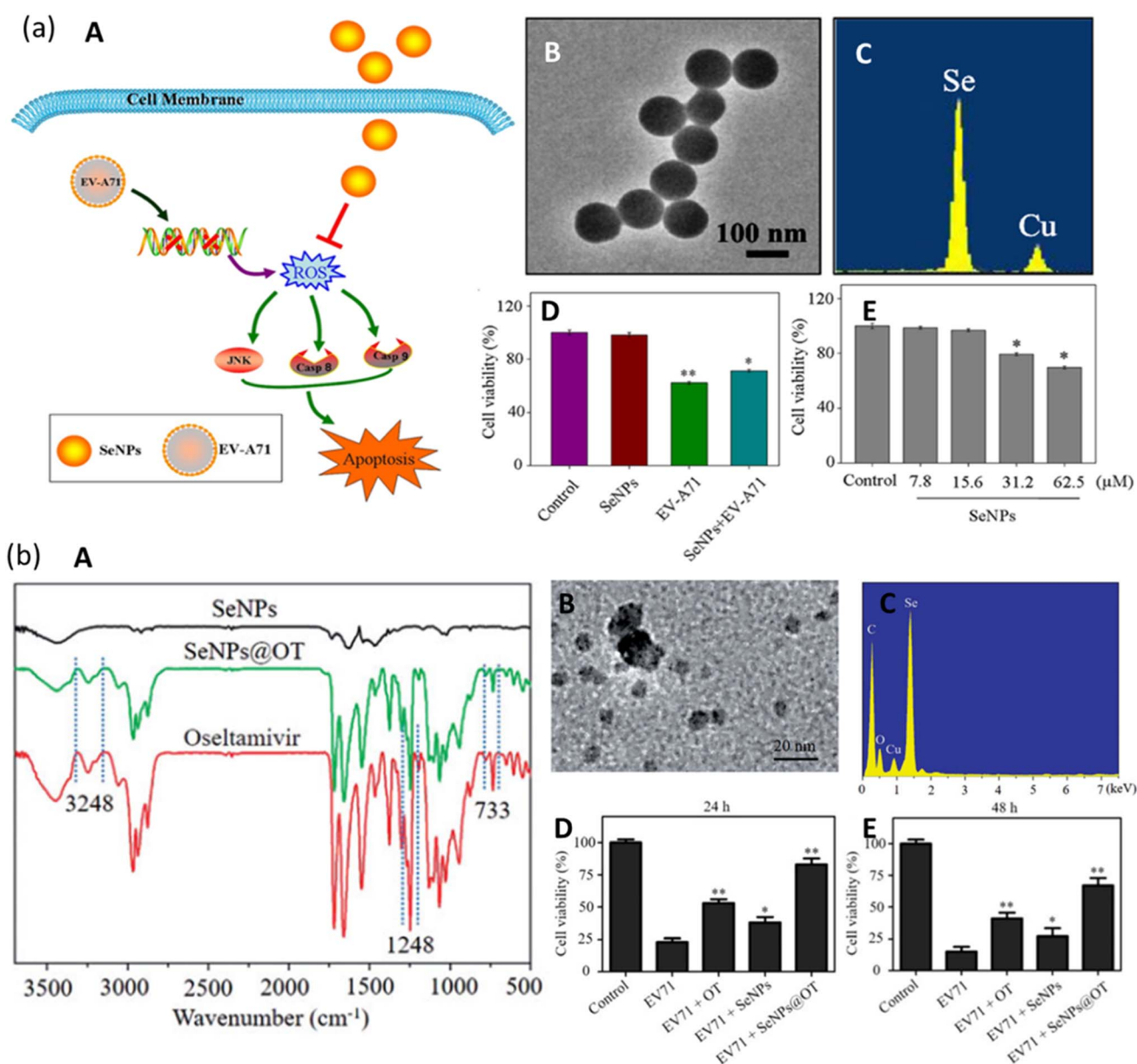


Fig. 7 (a) Mechanism of JNK and caspase signaling pathways. Green arrows show direct stimulatory modifications while orange shows direct inhibitory modifications (A). TEM micrographs of SeNPs (B). EDX pattern of SeNPs (C). MTT assay for antiviral activity (D). MTT assay for cell viability (reprinted with permission from ref. 46 Copyrights 2019 ACS). (a) FTIR spectrum of SeNPs, SeNPs loaded with OT and of OT (A). TEM micrograph of SeNPs@OT (b). EDX pattern of SeNPs@OT (C). Stability of SeNPs assessed in aqueous solution (D) and in PBS (E) (reprinted with permission from ref. 50 Copyrights 2019 Taylor and Francis Group).





Table 1 Antiviral activity of different metallic and functional nanoparticles against a broad spectrum of viruses along with key parameters reported

Nanoparticle(s)	Virus	Classification of virus	<i>In vitro</i> or <i>in vivo</i>	Size (nm)	Synthesis method	Mechanism	Reference
Ag <sub>2</sub> O/AgO-NPs and Au-NPs	Herpesvirus	HSV-1	<i>In vitro</i>	14.42–48.97 nm [Ag <sub>2</sub> O–AgO-NPs]; 15.60–77.13 nm [Au]	Biosynthesis	—	20
Ag <sub>2</sub> S nanoclusters	Coronavirus	Porcine epidemic diarrhea virus (PEDV)	<i>In vitro, in vivo</i>	3.7 nm and 5.3 nm	One-pot method	Prevents synthesis of viral negative-strand RNA and viral budding	51
AgNPs	Dengue virus	DENV	<i>In vitro</i>	100 nm	Biological (seed extract)	—	52
	Influenza	H3N2	<i>In vitro, in vivo</i>	9.5 nm	Oxidation-reduction method	Destruction of morphologic viral structures	24
		H1N1	<i>In vitro</i>	10 nm	—	—	23
		H1N1	<i>In vitro</i>	5–15 nm	Ultra-sonication method	—	22
	Enterovirus 71	EV71	<i>In vitro</i>	—	Simple method	—	17
	Respiratory syncytial virus	RSV infections	<i>In vitro, in vivo</i>	8–12 nm	—	Prevents entry of viral glycoproteins into the host cell	16
	Dengue virus	DENV	<i>In vitro</i>	30–70 nm	Biological (plant extract)	—	53
	Hepatitis	HSV-1, HAV-10 and CoxB4	Used design studio	8.91–27.89 nm	Biological (plant extracts)	—	21
	Herpesvirus	HSV-1 and HSV-2	<i>In vitro, in vivo, ex vivo</i>	13 to 54 nm	—	Affect viral attachment	19
	Pollivirus	PV	<i>In vitro</i>	7.1 nm	Electrochemical method	Cytopathic effect (CPE)	18
Au-MES NPs	Herpesvirus	HSV-1	—	4 nm [Au-MES NPs]	Solution-based method	Prevents virus from attaching, entering and spreading from cell to cell	54
AuNPs	Herpesvirus	HSV	—	~7 nm	Gallic acid in a bath sonicator	Prevents the attachment/penetration of virus	40
	Human immunodeficiency virus	HIV-1	—	1.7 nm and 2.6 nm	—	Binding to gp120	41
	Influenza	Influenza A viruses (IAVs)	—	2 nm and 14 nm	—	Multivalent interaction with sialic-acid-functionalized AuNPs	42
AuNPs interfering RNA	Dengue virus	DENV	<i>In vitro, in vivo</i>	12.92–43.25 nm	Chemical	Release infectious virion	43
Carbon dots NPs	Human immunodeficiency virus	HIV-1	—	2 nm	Pyrolysis of citric acid	Suppressing the syncytium formation	55
Carbon quantum dots (CQDs)	Highly pathogenic coronavirus	HCoV	—	7.6 ± 0.2 nm	Hydrothermal carbonization	—	56
Copper(I) iodide NPs	Influenza	H1N1	—	160 nm	—	OH <sup>-</sup> radicals are generated and viral proteins undergo degradation	57

Table 1 (Contd.)

Nanoparticle(s)	Virus	Classification of virus	<i>In vitro</i> or <i>in vivo</i>	Size (nm)	Synthesis method	Mechanism	Reference
	Feline calicivirus	FCV	—	100–400 nm	—	Cu <sup>+</sup> ions generated followed by protein oxidation	58
Copper-graphene (Cu-Gr) nanocomposite	Influenza	Influenza A viruses (IAVs)	—	—	—	Inactivate the virion particles within a half hour, preventing entry to the host cell	59
CuO NPs	Herpesvirus	HSV-1	<i>In vitro</i>	40 nm	—	Production of ROS <i>via</i> Cu <sup>+</sup> OR degradation of viral genome	60
Cuprous oxide NPs	Hepatitis	HCV	<i>In vitro</i>	45.4 nm	Solution phase	Inhibited entry of HCV pp	61
GO-Ag NPs	Feline coronavirus (FCoV); non-enveloped virus and infectious bursal disease virus (IBDV); Enveloped virus	FCoV and IBDV	—	5–25 nm	Hummers' method	—	39
Gold nanorod-based HR1 peptide	Coronavirus	SARS CoV-2	—	18 nm (diameter)	Chemical solid phase	Increases the immune indicators and decreases the inflammation indicators	62
Iron oxide NPs	Influenza	H1N1	<i>In vitro</i>	10–15 nm	Chemical reduction and magnetic separation	—	63
NiO nanostructures (NONS)	Cucumber mosaic virus	CMV	<i>In vivo</i>	15 to 20 nm	One-pot hydrothermal synthetic approach	Increase the expression of pod, pr1 and pal1 genes	26
Se@PEI@siRNA	Enterovirus 71	EV71	—	80 nm	—	Chances of SK-N-SH cells for staying in sub-G1 phase are reduced	64
SeNPs	Enterovirus 71	EV71	<i>In vitro</i>	10 nm	—	SeNPs@OT entered host cells by clathrin-associated endocytosis while suppressing EV71 proliferation	50
Ag NCs with SiO <sub>2</sub> composite sputtered coating	Enterovirus A71 Coronavirus	EV-A71 SARS CoV-2	— —	100 nm Less than 200 nm	Simple method Co-sputtering with argon at radio frequency	Cytopathic effect Coating possessed a virucidal effect	46 65
GO-Ag nanocomposite	Porcine epidemic diarrhea virus	PEDV	<i>In vitro</i>	17 ± 3.4 nm	Self-assembly <i>via</i> interfacial electrostatic force	Prevent entry of PRRSV to host cells	66
TiO <sub>2</sub> nanostructures (TDNS)	Broad bean stain virus	BBSV	—	—	Modified direct hydrothermal synthesis	Inducing systemic resistance	35
TiO <sub>2</sub> NPs	Influenza	H1N1 H3N2	— —	— 4–10 nm	— —	Strong oxidation effect Fragmentation of viral envelope	38 67







Table 1 (Contd.)

Nanoparticle(s)	Virus	Classification of virus	<i>In vitro</i> or <i>in vivo</i>	Size (nm)	Synthesis method	Mechanism	Reference
Tungsten carbide nanoparticles (WC NPs)	Poliovirus type-1, vaccinia virus ankara, human adenovirus type 5, Murine norovirus	PV-1, MVA, HAdV-5, MNV	<i>In vitro</i>	10–20 nm	Plasma atomization	—	68
Zirconia NPs	Influenza	H5N1	<i>In vivo</i>	200 nm	Two-step selective etching method Mechanical method	Promote the release of cytokines in mice Virus inhibited once it enters the host cell	27
ZnO NPs and PEGylated ZnO NPs	Influenza	H1N1	<i>In vitro</i>	20–50 nm ZnO-NPs; 16–20 nm ZnO-PEG-NPs			30

potential of AuNPs is not limited till here. Papp *et al.* have demonstrated in previous studies about the capability of AuNPs in the treatment of Influenza A Viruses (IAVs).<sup>42</sup> They showed that sialic-acid coated glycerol dendrons when immobilized on 14 nm AuNPs caused an appreciable anti-influenza effect. Moreover, AuNPs were non-toxic under operating conditions. The AuNPs have also been found compatible with the treatment of Dengue virus (DENV). For instance, Paul and his collaborators have reported that biocompatible AuNPs can be used to improve the delivery and stability of siRNA.<sup>43</sup> When entered Vero cells, they decrease DENV-serotype 2 replication to a great extent by releasing infectious virions. Hence AuNPs can be used for DENV infection control *in vitro*.

## 2.8 Selenium NPs

There are no effective drugs for the treatment of EV-A71. Selenium (Se) is present in our body as a nutritional element that is responsible for protection against viral infections. Recent studies have reported that SeNPs have excellent bioavailability and lower side effects due to their smaller size<sup>44,45</sup> and hence have the potential to be used as an antiviral agent against EV71.

Li *et al.* investigated the effect of SeNPs on the suppression of EV-A71 virus as they interfere with JNK signaling pathways.<sup>46</sup> As seen in Fig. 7a(A), the SeNPs can pass through the cell membrane and suppress the generation of Reactive Oxide Species (ROS) by EV-A71. They interfered with and successfully inhibited JNK signaling pathways by mechanisms of caspase-8 and caspase-9-mediated apoptosis in the cells infected by the virus. They synthesized SeNPs *via* a simple method and were able to prepare uniform NPs of size roughly 100 nm, as confirmed by the TEM micrograph in Fig. 7a(B). Due to their smaller size, SeNPs were highly stable and able to penetrate the cells. The presence of Se and Cu was confirmed in energy dispersive X-ray spectroscopy (EDX) as they form the SeNPs and the copper grid (Fig. 7a(C)). Thiazolyl blue tetrazolium bromide (MTT) assay was employed to examine the cell viability with SeNPs. Cell viability can be seen to slightly decrease in Fig. 7a(D). The decrease can be attributed to the concentration of SeNPs. This indicates that SeNPs can inhibit the EV-A71 virus proliferation. The MTT assay also measured the antiviral activity of SeNPs (concentration maintained at 15.625  $\mu$ M). The results show that cell viability was increased to 71% by SeNPs as compared to 59% when treated with EV-A71 virus (Fig. 7a(D)). This suggests good antiviral efficacy of SeNPs against EV-A71 virus.

For the treatment of EV-71 variant of enterovirus, oseltamivir (OT) is commonly used as an antiviral therapeutic agent. Although it has been approved for use by FDA, due to continuous usage, it has shown a decrease in antiviral efficacy.<sup>47</sup> To overcome this problem of inherent drug resistance against the virus, nanotechnology holds promise.<sup>48</sup> As discussed previously, Se is an important element in human body and hence its deficiency can result in increased susceptibility to virus infections.<sup>49</sup> Zhong *et al.* proposed a novel nanotechnological approach for increased antiviral efficacy against EV-71.<sup>50</sup> They fabricated a nano-sized functional antiviral system by loading OT on the

surface of SeNPs and evaluated its antiviral activity. The cell model for this particular study was chosen to be a human astrocytoma cell (U251). To confirm the chemical bonding between the drug and the NPs, Fourier transform infrared spectroscopy (FTIR) was performed whose graph is depicted in Fig. 7b(A). The spectrum is same as that of oseltamivir and peaks corresponding to 3248, 1248, and 733  $\text{cm}^{-1}$  can be seen for SeNPs@OT which is an indication of successful formation of a nano-sized antiviral system. The mean size of this nanosystem is confirmed by TEM micrograph in Fig. 7b(B), which confirms it to be around 10 nm. EDX results can also be seen in Fig. 7b(C), which shows characteristic peaks corresponding to Se (from NPs), O, and C (from OT) which further confirms the success in the preparation of SeNPs@OT. The cell viability of model U251 cells was examined and in Fig. 7b(D), the viability is lowest for EV-71 infected cells which increased to a greater amount with OT than SeNPs. However, when the prepared nanosystem SeNPs@OT was used, the viability of the infected cells was the highest. A similar experiment was conducted after 48 hours post infection and results can be seen to be similar as in Fig. 7b(E). Hence SeNPs loaded onto OT suppressed the cell apoptosis caused by EV-71 virus *via* mitochondrial pathway and reduced the generation of reactive oxygen species. Table 1 shows a summary of different metallic NPs which exhibit antiviral activity against a wide category of viruses along with their key parameters.

### 3. Nanoparticles for enhancing the efficacy of antiviral drugs

#### 3.1 Acyclovir

**3.1.1 Oral delivery.** Research is in progress to develop novel drugs for oral administration. Acyclovir (ACV) has issues of shorter half-life and poor permeability and hence patients' compliance is difficult. Mahmood *et al.* examined the effect of ACV in lipid polymeric particles and tested *in vitro* and *ex vivo*.<sup>69</sup> They aimed to enhance the controlled release of ACV *via* encapsulation with PEGylated Lipid Polymeric NPs. The NPs prepared *via* Box-Behnken Design (BBD) method were  $187.7 \pm 3.75$  nm in size. Polymers and amphiphilic molecules are widely employed for the effective delivery of hydrophilic and lipophilic molecules.<sup>70</sup> Their study aimed to develop a PEGylated lipid polymeric NP system by employing CS, lecithin, and PEG 2000 which was supposed to produce NPs with high encapsulation efficiency, easy permeability with sustained release profile. PEGylated ACV-loaded lecithin-CS NPs (PALNs) were synthesized and drug release parameters were assessed. The mechanism of formulation of PALN is schematically illustrated in Fig. 8a. Polar ACV attracts hydrophilic lecithin<sup>71</sup> which is followed by its addition to the CS solution. A stiff, stable nanostructure is hence obtained due to the formation of a CS shell around the NP.<sup>72</sup> PEG is used in applications of drug delivery as it gives stealth properties along with biocompatibility. It

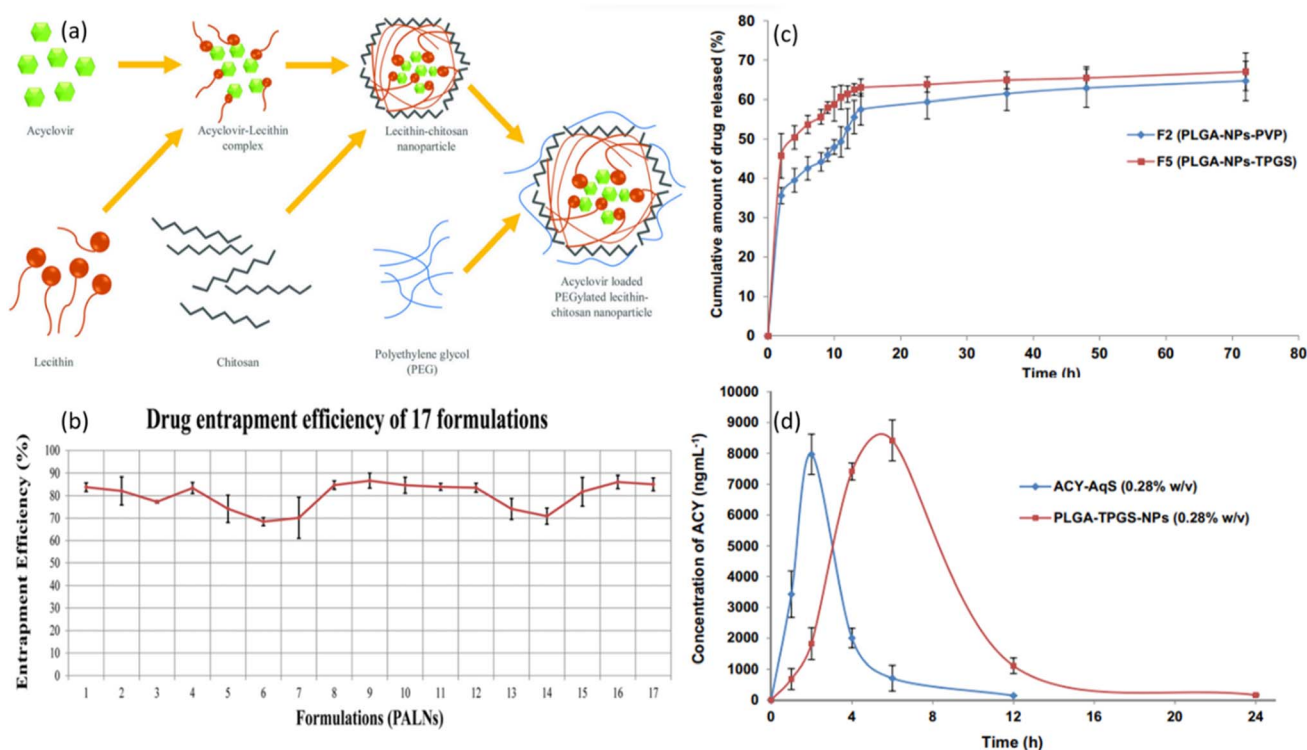


Fig. 8 (a) Schematic illustration of the mechanism of PALNs formation. (b) Graphical illustration of entrapment efficiency of 17 tested drug formulations (reprinted with permission from ref. 69 Copyrights 2020 AAPS). (c) *In vitro* release profiles of PLGA-NPs in STF with pH of 7.4. (d) The concentration of ACV in aqueous humor after topical ocular administration of formulation "F5" and ACV-AqS in eyes of rabbits (reprinted with permission from ref. 81 Copyrights 2018 Elsevier).



surpasses the immune system and enhances circulation time.<sup>73</sup> Its grafting was facilitated by interaction between nitrogen of amide group of CS and hydroxyl and etheric oxygen of PEG.<sup>74</sup> Good percentage entrapment was recorded for all 17 tested formulations as shown in Fig. 8b. The formulation was stable for up to 60 days and showed controlled release of drug for 24 hours.

Similarly, Saifi and her collaborators employed bilosomes nanocarriers (NCs) to enhance the oral bioavailability of ACV.<sup>75</sup> The *in vitro*, *ex vivo*, and *in vivo* assessments showed that a vesicle size of  $121.2 \pm 3.21$  nm was obtained *via* thin film hydration method (optimized *via* BBD) and showed 71.87–88.67% entrapment efficiency. The biocompatible bilosomes were found to be an effective drug carrier as they enhanced gut absorption of ACV at a considerably lesser amount dose than needed for a typical tablet.

**3.1.2 Ocular delivery.** Poorly soluble drugs are difficult to be administered *via* ocular route. Ocular bioavailability is markedly reduced due to the inherent anatomical and physiological barriers in eyes.<sup>76,77</sup> Despite the given constraints, ocular delivery is still a preferred route of administration. It was hypothesized that increasing the pre-corneal drug retention and enhancing its permeation can significantly improve the efficacy and bioavailability of these drugs.<sup>78</sup> Therefore, using NP-based delivery system could prove effective in overcoming the limitations associated with ocular delivery. Alkholief *et al.* employed biodegradable and biocompatible PLGA polymer stabilized with TPGS nanosystem for delivery ACV topically through eyes.<sup>81</sup> One of the major considerations while developing a polymeric NP system for ocular delivery is the biodegradation of polymer and its subsequent drug release profile. *In vitro* release profile was monitored for two optimized ACV formulations as shown in Fig. 8c. A biphasic release pattern is observed which shows an initial burst release for nearly 8 h followed by a controlled release for 14 h and subsequent sustained release for 72 h. ACV release was not governed by the percentage of PLGA but rather by the types of stabilizers used. The initial burst release may be due to PLGA undergoing biodegradation which causes drug attached to the surface to contact the medium and quickly solubilizes as a result.<sup>79</sup> The concentration of ACV was detected at regular intervals in rabbit eyes as shown in Fig. 8d. ACV-AqS and PLGA-TPGS-NPs were administered topically to the eyes of rabbits. For rabbits treated with ACV-AqS, ACV concentration could not be detected after 6th hour. The rapid corneal and precorneal loss might have played role in ACV not being able to be detected. In contrast, PLGA-TPGS-NPs treated rabbits showed detectable ACV concentration up to 24th hour, indicating a potential for nanosystem for sustained release of ACV and hence its increased efficacy. The authors reported that PLGA-TPGS-NPs ability to fight ocular viral infections is yet to be confirmed, however, they are a promising candidate for efficient delivery of ACV to the eyes.

Poorly soluble drugs can be employed for ocular delivery if their resulting eye irritation is under tolerance. The approach employed by Suwannoni *et al.* examined the ocular delivery route of ACV-loaded with BSA NPs which were surface modified with transactivating transduction (TAT) peptide, to deal with viral-

related keratitis.<sup>80</sup> About 200 nm-sized NPs showed less cytotoxic effects on HCE-T cells and resulted in the greatest ACV permeation in NPs. *In vitro* study showed that a novel formulation can be used for effective trans-corneal delivery of ACV.

**3.1.3 Intravenous delivery.** Vedula and his group employed precipitation method to prepare a formulation of ACV-carboxymethyl cellulose acetate butyrate NPs to overcome the inherent limitation of poor water solubility of ACV and to increase its efficacy in treatment of HSV.<sup>82</sup> The *in vitro* study showed that particle size of formulation was between 125–450 nm which was administered *via* intravenous route. The results demonstrated drug loading efficiency of about 40% and 9.2 wt% of the ACV was successfully loaded into nano carriers. This shows the potential of NPs not only in effective drug entrapment but also in an improved dissolution of ACV with around 10 times more release than pure ACV. The authors called for a need for more investigation to evaluate the long-term stability of NPs.

## 3.2 Efavirenz (EFV)

**3.2.1 Intravenous/intranasal delivery.** Many ARVs are unable to completely eradicate HIV *via* CNS targeting and hence chitosan-g-HPbCD NPs of EFV were developed.<sup>83</sup> Belgamwar *et al.* prepared NPs of  $198 \pm 4.4$  nm size *via* mild ionic gelation technique. The results showed sustained release ( $99.03 \pm 0.30\%$  in 8 h), greater permeability, improved CNS bioavailability, high drug targeting percentage, and entrapment efficiency of  $38 \pm 1.43\%$ . The *in vivo* results of intravenous (i.v.) and intranasal (IN) administration to mice are shown in Fig. 9.

**3.2.2 Oral delivery.** Nano-delivery systems are a viable option to increase the therapeutic efficacy and reduce the side effects of drugs that show poor water solubility. The study by Hari *et al.* evaluated the effects of using a nano-delivery system for EFV on its bioavailability, distribution, and effectiveness. Eudragit E100 was used to prepare polymeric NPs of size 110 nm by emulsion solvent evaporation method and showed impressive 99% entrapment efficiency.<sup>84</sup> Another group led by Kumar formulated EFV-loaded Lf NPs for oral delivery *via* sol-oil protocol and achieved a particle size of 45–60 nm.<sup>85</sup> They demonstrated that EFV-Lf NPs showed 2× times improved anti-HIV-1 action compared to free EFV and enhanced the oral bioavailability and *in vivo* pharmacokinetics profile. The formulation was also free from any toxicity issues.

## 3.3 Zidovudine (AZT)

**3.3.1 Intravenous delivery.** AZT is an extensively used anti-HIV/AIDS drug but has an inherent shorter half-life, low aqueous solubility, and is stopped by physiological barriers which have limited its use for intravenous administration. It is worth mentioning the study of Joshy *et al.* which investigated a nanosystem composed of dextran and stearic acid for effective delivery of AZT.<sup>86</sup> They were able to synthesize NPs of three different formulations ranging from size 356 nm to 730 nm *via* double emulsion solvent evaporation method. NPs were found to be highly effective in delivery of AZT as they showed entrapment efficiency as high as about 93%. Another approach





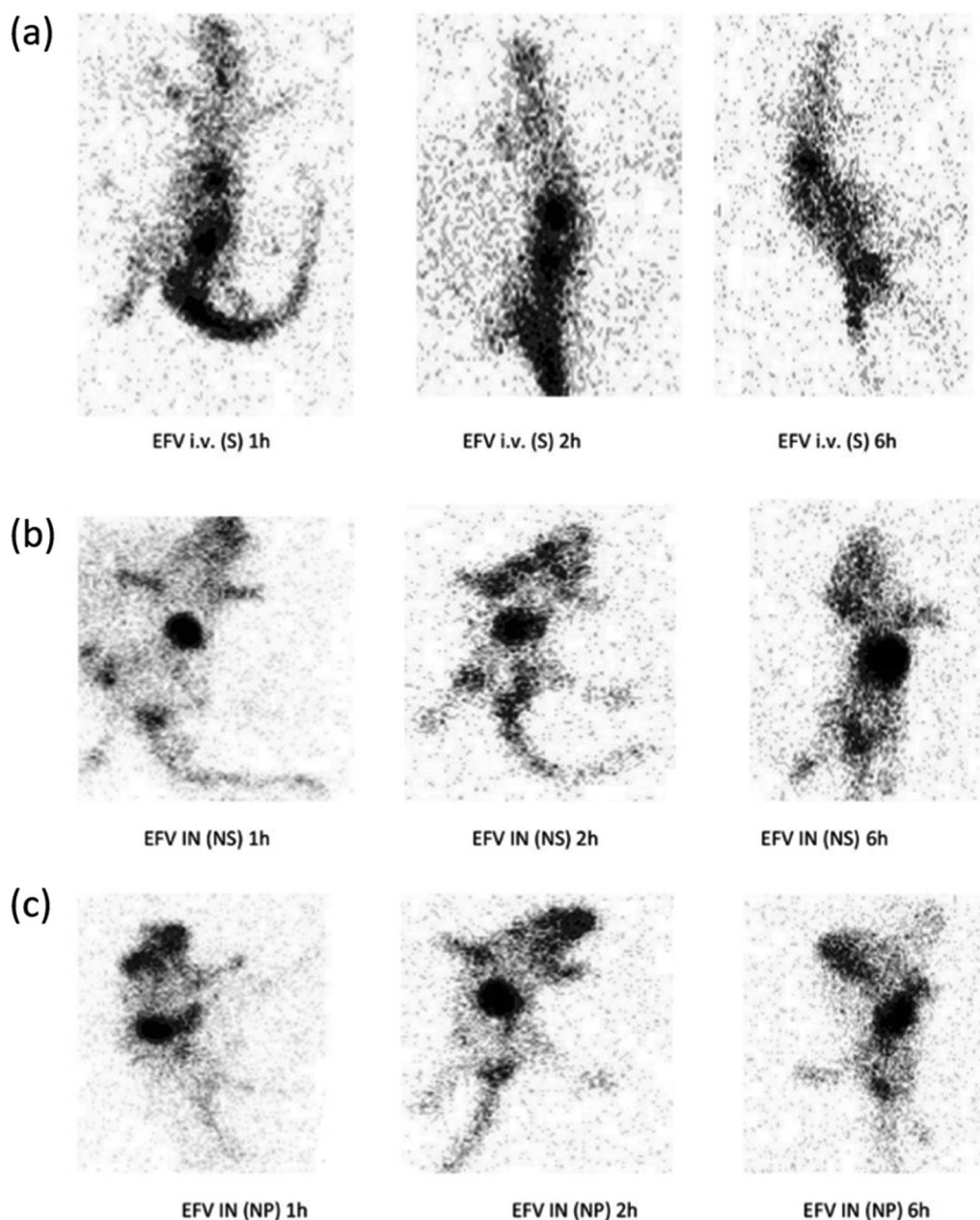


Fig. 9 Gamma scintigraphy images of rats showing the presence of radioactivity post-administration of intravenous efavirenz solution [EFV i.v. (S)], intranasal efavirenz solution [IN EFV (S)] and intranasal efavirenz nanoparticles (IN EFV-NPs). (a) EFV-i.v. (S), (b) EFV IN (S) and (c) IN EFV-NPs (reprinted with permission from ref. 83 Copyrights 2019 Taylor and Francis Group).

used AZT loaded with polyvinylpyrrolidone (PVP)/stearic acid (SA)-polyethylene glycol (PEG) nanoparticles (PSNPs) to address the shortcomings of AZT.<sup>87</sup> A similar synthesis method was used, and NPs of mean size  $341 \pm 4.34$  nm were obtained. Out of three different formulations of PSNPs, the highest encapsulation efficiency shown was about 96% with roughly 79% drug loading capacity. Considerably high cellular internalization was recorded which indicates its *in vivo* potential. Their group also evaluated AZT-loaded with amide functionalized alginate NPs, prepared *via* the same route.<sup>88</sup> The novelty of this work was the preparation of NPs without chemical crosslinking. The particle size was considerably higher *i.e.*, about  $432 \pm 11.9$  nm, and

showed a loading efficiency of  $29.5 \pm 3.2\%$ . The system was biocompatible, showed sustained release, and hence can be incorporated as drug carriers for intravenous administration of AZT.

**3.3.2 Oral delivery.** Joshy's group also developed biocompatible, safe, and stable lipid NPs modified with polymer gelatin loaded as carriers of AZT, prepared *via* modified double emulsion solvent evaporation method.<sup>89</sup> The prepared nanocarrier system showed appreciable loading, controlled release profile, and good compatibility with blood. Encapsulation efficiency of  $87.4 \pm 0.58\%$  was confirmed *in vitro*. Hence oral or topical route of administration is preferred for prepared formulation.



The ideal approach for treating many diseases by using the same delivery system is to employ multi-functional NPs. In another study, they prepared hybrid NPs of carboxy methyl cellulose–AZT core enclosed by a Compritol (Comp)–polyethylene glycol shell.<sup>90</sup> *In vitro* study results showed that the system was biocompatible, cytocompatible, and showed appreciable loading coupled with controlled release of AZT drug and encapsulation efficiency of 82%. The results open doors for more opportunities for the development of LPNs as an efficient delivery vehicle of antiviral drugs.

**3.3.3 Transdermal delivery.** Two colloidal carrier systems (microemulsion (ME) and lamellar phase (LP) liquid crystal) were investigated for drug permeation capacity.<sup>91</sup> Both *in vitro* and *in vivo* studies were conducted to examine the efficacy of the proposed system. The results showed ME showed 2 times higher permeation effect with tolerable skin irritation as evaluated *in vivo*. Hence ME proved to enhance permeation of drugs and cause negligible irritation to the skin.

**3.3.4 Possible routes for aloe vera based administrations.** Joshy and his collaborators developed AZT-loaded solid lipid nanoparticles (SLNs) of stearic acid (SA) modified with aloe vera gel *via* simple emulsion solvent evaporation method.<sup>92</sup> The formulation was  $265.61 \pm 80.44$  nm in size. The prepared system holds good stability at room and refrigerated temperatures. The study examined the SLN particles *in vitro* profile and showed enhanced growth and proliferation of cells without exhibiting any toxicity with an encapsulation efficiency of  $74.92 \pm 1.2\%$ . The proposed combination can be used as an effective tool for the treatment of HIV.

Previous research has shown that *Aloe vera* can be administered to patients *via* oral, transdermal, and buccal drug delivery.<sup>93</sup> However, all these delivery routes for the application of *Aloe vera* gel have corresponding setbacks. For instance, when administered through oral route, although it is much easier for patient to intake the drug, however, drug

administration is associated with poor bioavailability coupled with low absorption of proteins.<sup>94</sup> An alternate to oral delivery, buccal route of administration has been researched extensively.<sup>95</sup> A major drawback of buccal administration is the need for permeation enhancers which if absent would limit membrane permeation of some compounds across cheek mucosa and therefore cause unsuccessful delivery of *Aloe vera*. But perhaps the most effective route for administration, according to our perspective, is applying *Aloe vera* drug *via* skin or transdermal route. It has many positive outcomes associated which include but are not limited to successful avoidance of first-pass metabolism, comparatively and adequately greater surface area for absorption, less frequent doses required and its inherent noninvasive nature.<sup>96</sup> We suggest more research should be conducted on exploring the nanocarriers systems for achieving synergistic effects of *Aloe vera* gel and nanoparticles used for its transport to treat viral infections.

### 3.4 Lopinavir (LPN)

**3.4.1 Oral delivery.** Treatment of various diseases such as HIV and tuberculosis needs the administration of multiple drugs. Hence fixed-dose combinations were developed for adults which were in the form of tablets and capsules. The lack of child-friendliness of those adult formulations pushed the pharmacists to break the tablets and open the capsules. However, due to preservatives, bitter taste, low solubility, and stability associated with it, the practice lacked standardization with inaccurate doses and reduced clinical efficacy.<sup>97,98</sup> WHO recommended developing sachets and mixing them with liquids or adopting alternatives such as sprinkles to pour over food and tablets which quickly disintegrates once in mouth.<sup>99</sup> Novel approaches are hence required to develop pediatric formulations for drugs that show poor aqueous solubility. Pham *et al.* proposed employing nanotechnology to synthesize

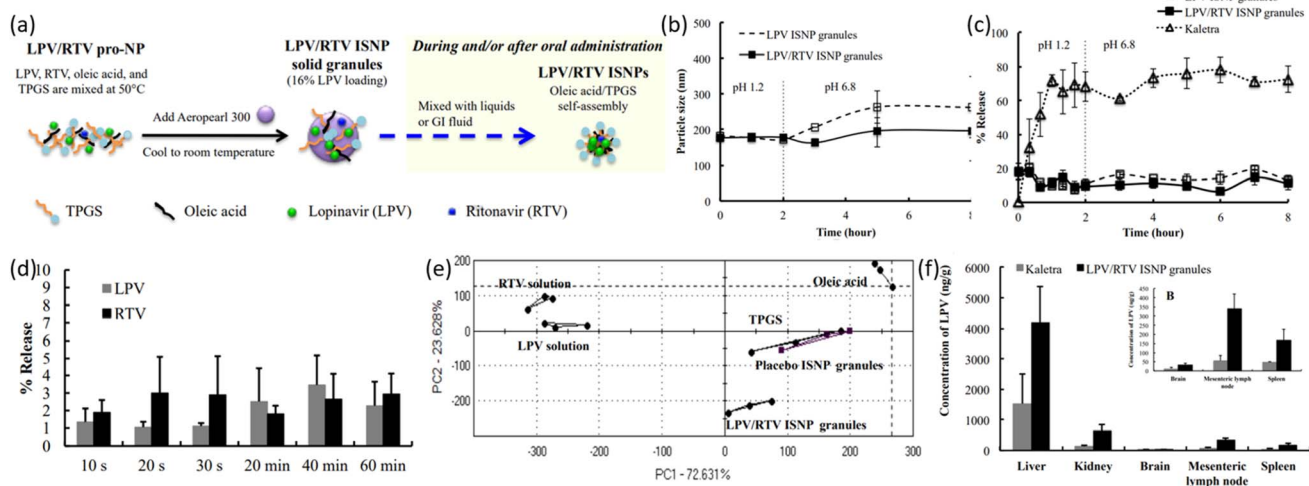


**Fig. 10** (a) Schematic illustration of LPV/RTV ISNP granules preparation and LPV/RTV ISNPs formation. (b) Physical stability of LPV/RTV ISNP granules and LPV ISNP granules in physiological conditions (simulated). (c) Dissolution profiles of LPV from LPV ISNP granules and Kaletra. (d) Taste examination of LPV/RTV ISNP granules in PBS maintained at pH 6.8 and (e) using an Astree e-tongue. (f) Distribution of tissues by LPV after oral administration to rats (reprinted with permission from ref. 100 Copyrights 2016 Elsevier).



*in situ* self-assembly NPs (ISNPs).<sup>100</sup> They prepared a fixed-dose combination of ART drugs namely lopinavir (LPV) and ritonavir (RTV) ISNP granules as well as LPV ISNP granules *via* warm microemulsion precursors (with modification). The formulation had a size of about 158 nm which resulted in 95% entrapment efficiency for both drugs with 8 hours of stability. Fig. 10a schematically illustrates the preparation method for LPV/RTV granules and ISNPs. Both LPV and RTV were able to entrap in the ISNPs as soon as granules were introduced to water. Moreover, method of preparation is quite simple as it requires only one mixing step to give ISNP granules loaded with drugs having excellent flow properties. The physical stability of LPV and LPV/RTV ISNP granules was assessed in 37 °C physiological conditions. An 8 hour analysis of particle size did not show any apparent change in particle size. This essentially implies that prepared formulations of ISNPs are not affected by changes in pH, temperatures, and ionic strength. The graph of particle size against time (in hours) is shown in Fig. 10b. The dissolution profile was recorded by performing a two-stage dissolution test to monitor the release of LPV from LPV ISNP granules and LPV ISNP granules from LPV/RTV ISNP granules as shown in Fig. 10c. The initial burst release of LPV can be attributed to LPV attached on the surface of LPV, while sustained release afterwards is a result of good entrapment of LPV inside ISNPs. The release profile of LPV/RTV granules is quite like LPV ISNP granules which implies that incorporation of RTV did not affect the released of LPV. Efficacy of taste-masking was proven from results of Fig. 10d, where about 3% of LPV and RTV were released over a period of 1 hour at pH of 6.8. To further verify these results Astree e-tongue method was used. By comparing the distance between the Euclidean from formulations on placebo, taste of prepared formulations was examined. As shown in Fig. 10e, the cluster of LPV/RTV ISNP granules is closer to the placebo ISNP granules than LPV and RTV solutions which indicates effective taste-masking ability of ISNP granules. The results of biodistribution studies shown in Fig. 10f indicates that LPV concentration is fairly increased in liver, kidney, brain, lymph nodes and spleen. These results collectively indicate good potential of ISNP granules in overcoming bad taste of LPV and RTV drugs while exhibiting high entrapment efficiency and achieving pediatric compliance at large. The nanotechnology can be used to formulate a fixed-dose specification of drugs which are poorly water-soluble and are meant to be taken by children who must take multiple drugs for HIV treatment. This would reduce the pill burden and achieve increased children compliance.

Ravi and Vats prepared SLNs-LPV formulation for enhanced HIV action by increased oral bioavailability, evaluated *in vivo* with a rat model.<sup>101</sup> They employed warm oil-in-water (O/W) micro-emulsion technique and prepared NPs of  $196.5 \pm 3.5$  nm size. Entrapment efficiency of  $76.5 \pm 3.5\%$  was recorded. Another study also reported SLN-LPV formulation prepared *via* hot self nano-emulsification (SNE) method which achieved  $180.6 \pm 2.32$  nm NP size and entrapment efficiency of  $91.5 \pm 1.3\%$ .<sup>102</sup> The results showed higher oral bioavailability and lymphatic drug transport. The novel synthesis method of SLN

preparation was explored and can be used for the preparation of SLNs of higher fatty acids.

Another novel method for enhancing the oral delivery of LPV *via* Pullulan Acetate NPs was explored by Ravi *et al.* by employing Motozato's method and achieving a particle size of nearly 197 nm.<sup>103</sup> The prepared formulation was quite effective in the treatment of HIV infections by using LPV as an antiviral drug and pullulan acetate NPs as nanocarriers which enhanced the oral bioavailability and hence the effectiveness of the formulation against HIV. The bioavailability of LPV from NPs was about 2× greater compared to free LPV. Higher distribution of LPV-loaded NPs to lymphoid organs was recorded with an entrapment efficiency of 75%.

### 3.5 Saquinavir (SQV)

**3.5.1 Oral delivery.** SQV has inherent poor water solubility and thus has poor antiviral activity. For enhancing its antiviral efficacy, bioavailability, and biodistribution, Dodiya *et al.* incorporated SLNs into SQV.<sup>104</sup> They used hot high-pressure homogenization (HPH) method for the preparation of  $215 \pm 9$  nm [SQSLNs NPs] and  $344 \pm 16$  nm [SNS NPs]. The results showed that bioavailability was increased to 37.39% [SNS] and 66.53% [SQSLN] from 18.87% of SQV micro-suspension. Enough drug was able to entrap as entrapment efficiency of  $79.24 \pm 1.53\%$  was reported. The antiviral drug used was SQV and the nanosuspensions were of SQV too. The *in vivo* studies showed greater plasma level concentration than SMS. Thus, SLNs and nanosuspensions are promising candidates for the enhancement of oral bioavailability of drugs that exhibit poor aqueous solubility. A large fraction of drugs suffer from issues of poor aqueous solubility and low bioavailability. Studies have shown that nano-sized formulations have proven to be effective in overcoming this problem, as discussed above.

Yuan *et al.* examined the result of employing nanocrystal suspension on the oral bioavailability of SQV.<sup>116</sup> Nanocrystals of SQV were prepared *via* the anti-solvent precipitation-high pressure homogenization method. The size of nanocrystals was  $205.93 \pm 3.74$  nm having a narrow poly-dispersity index (PDI) of 0.1. The nanocrystals were hence uniformly distributed. The zeta potential showed a high negative value which is a representation of the good stability of the prepared formulation. The rod-shaped particles were confirmed from TEM micrographs. Fig. 11a shows the results of the cellular uptake study performed on Caco-2 cells. The higher fluorescent intensity of SAQ nanocrystals indicates high drug uptake in cells. Small red dots seen in the cytoplasm of cells after 2 h could potentially be the SQV nanocrystals. In contrast, there are only a few particles observed in the cytoplasm of SQV coarse crystals after a similar 2 h period and at the same level of excitation intensity. The level of fluorescence intensity after 0.5, 1, and 2 hours of SQV nanocrystals can be seen to be significantly higher than SQV coarse crystals which are in line with increased cellular uptake of nanocrystals in Caco-2 cells, as shown in Fig. 11b. The better cellular uptake profile of SQV nanocrystals can be linked to their lower crystallinity. As shown in Fig. 11c, SQV nanocrystals and coarse powder exhibit similar





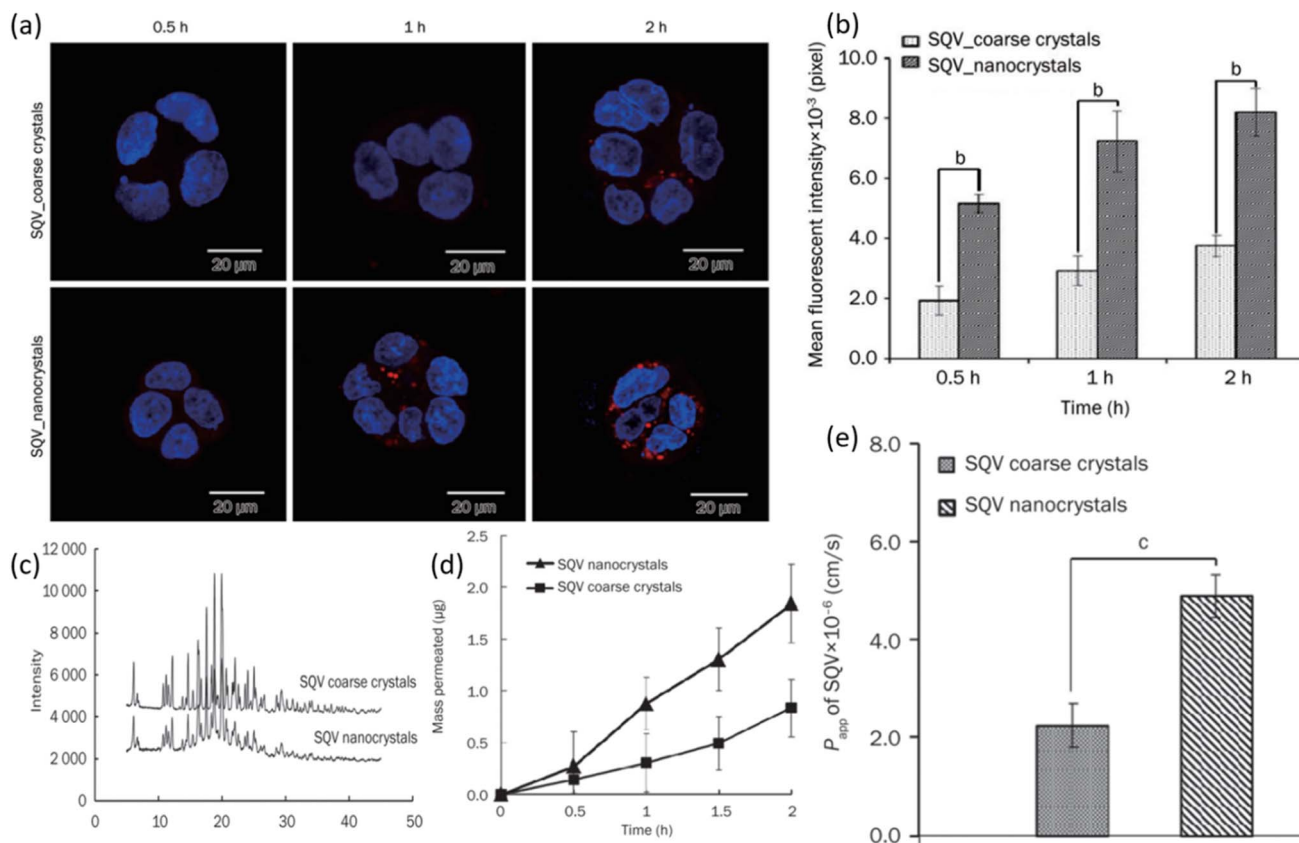


**Fig. 11** (a) Cellular uptake of SQV coarse and nanocrystals was observed *via* laser scanning microscope. (b) The fluorescence intensity of cells was analyzed quantitatively. (c) XRPD diffraction pattern of SQV coarse and nanocrystals. (d) Permeation profiles of SQV through a monolayer of Caco-2 cells and (f) permeability coefficient of SQV across monolayers (reprinted with permission from ref. 106 Copyrights 2015 Nature).

degrees of crystallinity. The drug release study was performed on both coarse and nanocrystals. After a period of 2 h, roughly 20% coarse crystals were able to dissolve compared to 60% dissolution of nanocrystals. As expected, the dissolution of nanocrystals is much quicker than coarse crystals of SQV. A similar experiment was performed by monitoring the release profile of ethyl rhodamine B (RHD) from both coarse and nanocrystals. Release profiles exhibited a similar pattern as before with a greater percentage release from SQV nanocrystals. The RHD was entrapped in the crystal lattice of SQV nanocrystals and showed immediate release once nanocrystals dissolved. The effect of particle size of SQV on the drug transport across the Caco-2 cells monolayer from apical (AL) to basolateral (BL) side was assessed. As seen in Fig. 11d, the percentage of SQV in the receiving chamber (BL side) is increasing as time progresses. Yet again, a greater percentage of drug was able to pass through the monolayers when they were treated with nanocrystals, hence indicating faster drug transport for SQV nanocrystals than coarse crystals. The apparent coefficient of permeability ( $P_{app}$ ) of SQV was determined by treating Caco-2 cells with both formulations. The greater permeability of SQV nanocrystals is seen as shown in Fig. 11e. All these results together indicate that SQV nanocrystals have enhanced oral drug absorption. A recent study by Krieser and her group aimed to improve the taste masking and stability of

the SQV nanostructures developed for enhanced pediatric adherence.<sup>105</sup> They employed interfacial polymer technique and prepared SQV NPs of 136–158 nm average diameters. The prepared formulation exhibited sustained release, a high drug loading capacity of 80%, ability to encapsulate 97% of the drug with low dynamic viscosity. The *in vitro* studies showed that SQV NPs showed excellent stability and controlled release properties. The dose can be given in a liquid form to the children with a taste acceptable to them. This amounts to an appreciation for designing drug delivery systems to treat children suffering from HIV.

### 3.6 Indinavir (IDV)

**3.6.1 Oral delivery.** The use of biodegradable polymeric NPs for improved oral delivery is a unique approach. Indinavir is an anti-HIV agent which has limited aqueous solubility. The study reported increased drug loading and EE of the proposed system.<sup>107</sup> The strategy employed was the preparation of mPEG-PCL NPs to enhance bioavailability and increase aqueous solubility. They reported emulsification solvent evaporation method to prepare the NPs with an average size of  $211 \pm 10.12$  nm. At a pH of 1.2 (PBS) after 96 hours, 60% drug release was recorded. The developed copolymer can self-assemble into NPs and has good drug loading and entrapment efficiencies.



The results from *in vitro* studies show that mPEG-PCL and IDV system shows initial burst release which is then followed by sustained release. On other hand, *in vivo* studies showed that the drug administered to rat *via* oral route show an increase in plasma concentration, and appreciable cellular uptake by Caco-2 cell line with improved circulation was also reported. Hence a novel strategy was explored by using biodegradable polymeric NPs, surface modified to enhance oral bioavailability.

To treat children suffering from HIV, the dose being administered to them *via* oral route must be taste-masked and in liquid form to prevent difficulties in swallowing the tablets. A study reported the preparation of  $155 \pm 7$  nm size NPs of formulation of Monoolein and IDV, using magnetic stirring and high-pressure homogenization method.<sup>108</sup> The incorporation efficiency of the formulation was 96% and IDV was able to remain in the same concentration for a month while exhibiting a sustained release profile. This combination was not only biocompatible but showed no irritation with improved taste-masking and the ability to overcome the bitter taste of the drug. Thus, it can be used for pediatric HIV treatment.

**3.6.2 Intravenous delivery.** One of the shortcomings of the IDV drug is that it has limited effectiveness in inhibition of virus due to efflux by P-gp at BBB. Employing Tween 80 containing LNEs for enhancing the delivery of IDV to brain was shown to be a viable strategy.<sup>109</sup> *In vivo* studies show that brain uptake in

mice was considerably improved. Further studies may prove IDV effectiveness in the reduction of viral load in brain.

### 3.7 Lamivudine

Glycyrrhizin LMW CS NPs can be used as an effective drug carrier system for liver targeting with decreased damage to tissues and sustained release of the drug. Glycyrrhizin has demonstrated antiviral activities against a broad spectrum of viruses.<sup>110,111</sup> Chitosan is a non-toxic, biocompatible, and biodegradable polymer that is widely used as a carrier molecule for various vaccines, genes, protein molecules, *etc.*<sup>112–116</sup> Mishra *et al.* investigated the controlled release of GL conjugated LMW CS-NPs in liver targeting. Model drug lamivudine was encapsulated within GL-CS-NPs and intravenously administered to a mouse to examine the targeting efficacy. Conjugation of GL was determined by FTIR spectrum as shown in Fig. 12a. The amino functionality ( $-\text{NH}_2$ ) of CS has caused stretching of N-H at wave numbers  $3346 \text{ cm}^{-1}$  and  $3371 \text{ cm}^{-1}$  in Fig. 12a(A) and hence this spectrum is of CS-NPs. While in Fig. 12a(B),  $-\text{NH}$  deformation of  $-\text{NH}-\text{CH}_2$  verifies the successful conjugation of GL with an amino group in NPs and hence this spectrum represents GL-CS-NPs. *In vitro* release profile of lamivudine from NPs was examined in PBS solution maintained at a pH of 7.4. The *in vitro* study showed that CS-NPs were able to release  $59.2 \pm 2.1\%$  while GL-CS-NPs exhibited  $42.9 \pm 1.8\%$  release of lamivudine after 72 hours. It is obvious from the graph that the

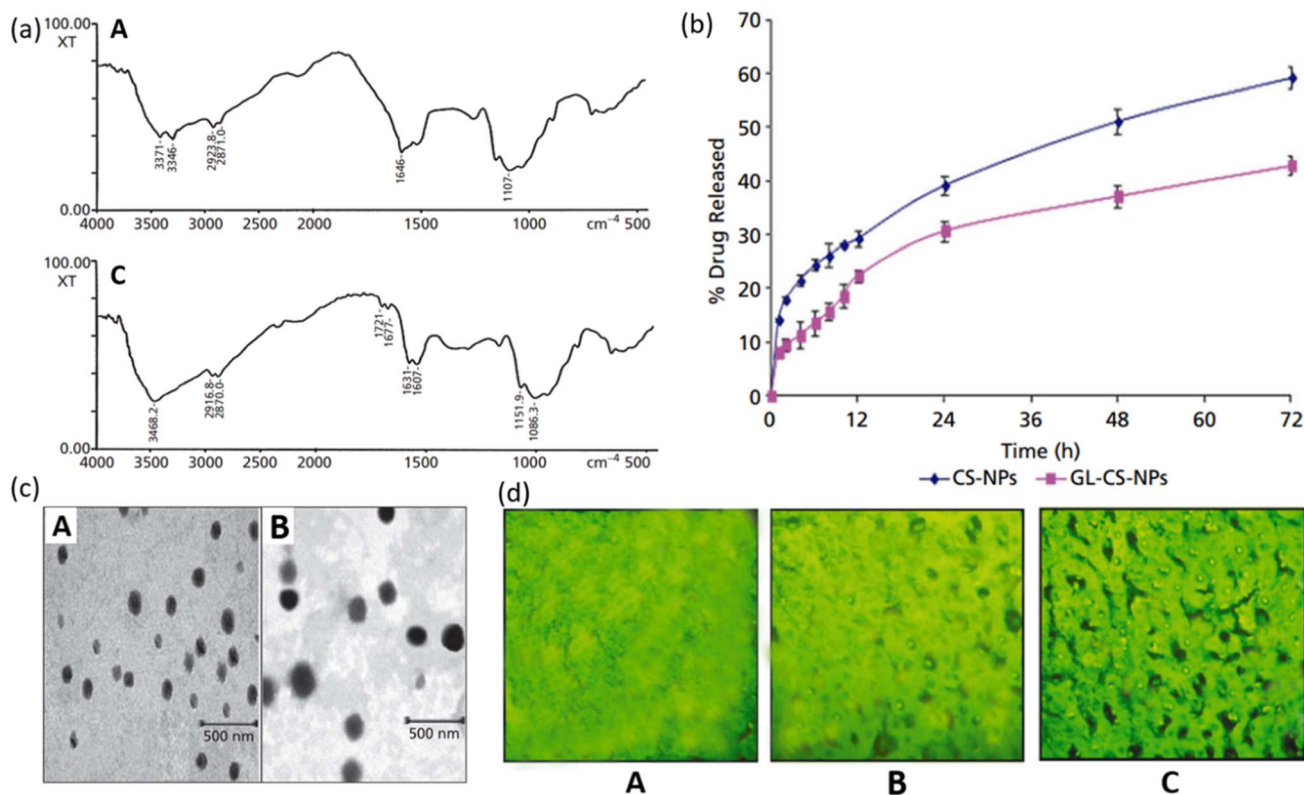


Fig. 12 (a) FTIR spectrum of (A) CS-NPs and (B) glycyrrhizin conjugated LMW CS-NPs. (b) TEM micrographs of (A) CS-NPs and (B) glycyrrhizin conjugated LMW CS-NPs. (c) Fluorescent photograph of FITC-labelled (A) plain drug solution; (B) CS-NPs; (C) glycyrrhizin conjugated LMW CS-NPs in the liver sac (reprinted with permission from ref. 117 Copyrights 2014 Wiley).

release profile showed a biphasic fashion, with an initial burst followed by a sustained release. The reason for initial burst release can be the attachment of drug particles on the surface of NPs. Lower drug release from GL-CS-NPs can be attributed to the presence of structural features which could have resulted in a double barrier effect. The TEM micrographs showed a smoother surface for CS-NPs than GL-CS-NPs which can be due to the substitution of  $-\text{NH}_2$  of LMWC by GL (Fig. 12b). The fluorescence micrograph of GL-CS-NPs showed a higher accumulation of hepatocytes cells than plain dye solution and dye-loaded CS-NPs. The fluorescence image of the liver shown in Fig. 12c shows that GL-CS-NPs were able to localize preferentially in the liver and hence greater percentage of lamivudine was seen in hepatocyte tissues with GL-CS-NPs as compared to plain drug. The results of the study indicate that loading lamivudine in GL combined with LMWC-NPs improves the resistance time and quantity of drugs in the liver. This can lead to a reduction in the dosage and quantity of each dose. Moreover, hepatic targeting and controlled release can decrease the toxicity associated with lamivudine. Hence, liver targeting *via* controlled release of GL-CS NPs can be an effective strategy for the treatment of HIV.

Another route employed the hot homogenization method to produce lamivudine-MLN (multiple lipid NPs) to enhance the oral administration of the formulation.<sup>118</sup> The size reached after the combination of the drug and the NPs was about 450 nm. The simulation studies indicate that around 1.3% of MLN-lamivudine would be released in 4 hours in gastric fluid. The

release profile showed sustained and controlled release for about 45 hours. The developed system can be applied as a topical drug or orally administered (after resuspension).

### 3.8 Tenofovir (TFV)

**3.8.1 Vaginal route.** Due to rising HIV cases, there is a need to develop nanotechnology-based microbicides for the effective prevention of HIV sexual transmission. Hence there is a need for the development of nanocarriers that can act as potential drug delivery vehicles to administer microbicides to the targeted site. Although topical pre-exposure prophylaxis (PrEP) with ARTs has been developed and showed appreciable results in the prevention of vaginal transmission of HIV, because of poor adherence by women undergoing clinical trials<sup>119</sup> and concerns of non-biocompatibility, there is a need for the development of optimized microbicides. Machado *et al.* proposed incorporating PLGA/SA nanocomposite inside the tenofovir drug and its subsequent incorporation in hydroxypropyl methylcellulose (HPMC)/PVA-based film.<sup>120</sup> Nanocomposite with a mean size of 127 nm, prepared *via* double emulsion/solvent evaporation method, showed a drug association efficiency of 50%. The characterization of these films was performed by SEM and EDS techniques. The NPs can be seen to be uniformly embedded in the thin film as even at reasonably good magnification aggregates of particles are not visible as shown in Fig. 13a(A). This result was further confirmed by fluorescence microscopic imaging in Fig. 13a(B) where no visible difference can be observed for the film fracture surface

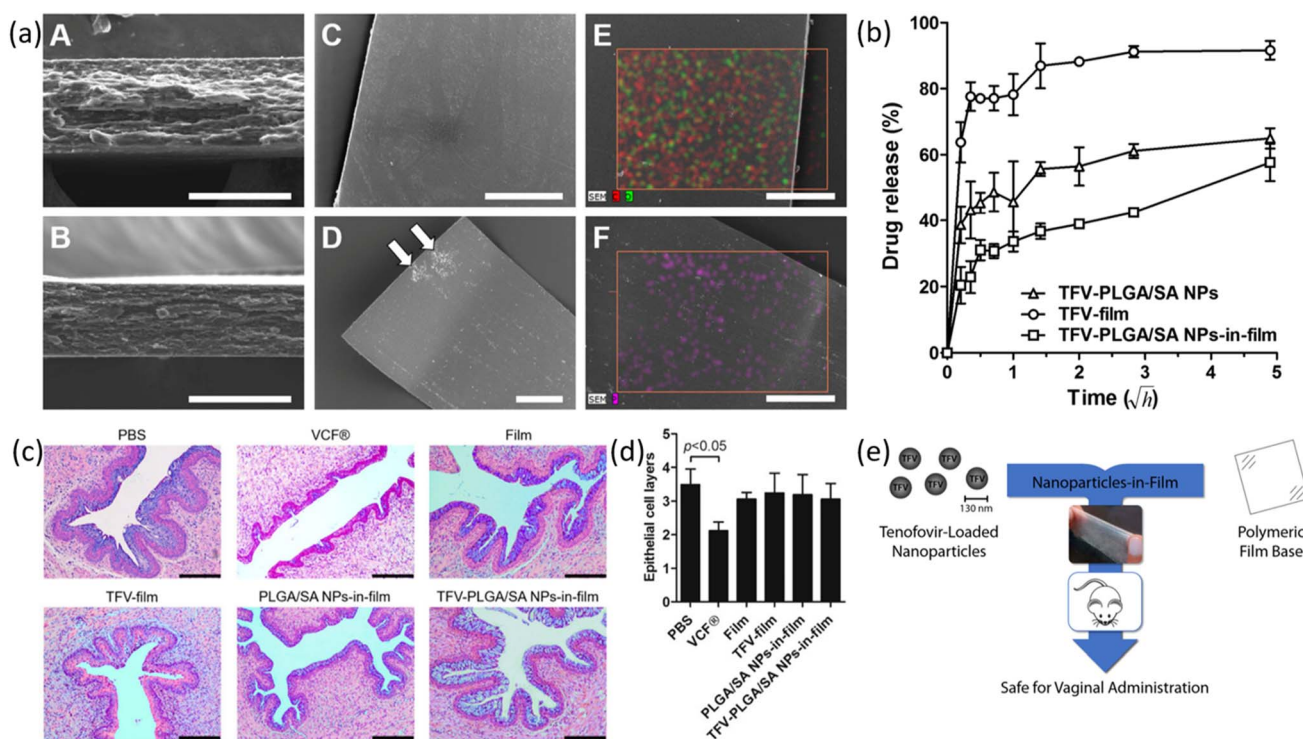


Fig. 13 (a) Characterization of films *via* SEM and EDS. (b) Drug release profiles for various films. (c) Analysis of H&E-stained vaginal mucosa (d) quantitative assessment of an average number of epithelial cell layers. (e) Schematic illustration of the proposed idea (reprinted with permission from ref. 120 Copyrights 2016 Elsevier).







**Table 2** Results of various studies over the past decade showing efficacies of different drug carrier systems with relevant parameters. (EE<sub>1</sub>: encapsulation efficiency, EE<sub>2</sub>: entrapment efficiency)

Antiviral Drug	Nanoparticle(s)	Action against virus	Route of administration	<i>In vitro/in vivo/ex vivo</i>	Size (nm)	Polydispersity index [PDI]	Synthesis method	Efficiency	Reference
Acyclovir	SILNs	[HSV]-TK	—	<i>In vitro</i>	180 nm	—	Emulsification and low-temperature solidification method	78% EE <sub>2</sub> %	124
	PEGylated lipid polymeric NPs	HSV-1 and HSV-2	Oral	<i>In vitro, ex vivo</i>	187.7 ± 3.75 nm	0.179 ± 0.03 to 0.429 ± 0.12	Box-Behnken design (BBD)	83.81 ± 1.93% EE <sub>2</sub> %	69
	Biosomes NCs	HSV-1, HSV-2, and varicella-zoster (VZV)	Oral	<i>In vitro, in vivo, ex vivo</i>	121.2 ± 3.21 nm	0.261 ± 0.023	Thin-film hydration technique. (Optimize by Box-Behnken statistical design)	71.87–88.67% EE <sub>2</sub> %	75
	Gel nanoemulsions (NEs)	HSV	Ocular	<i>In vitro, in vivo, ex vivo</i>	28 nm to 34 nm	0.38 ± 0.04 to 0.47 ± 0.05	Low energy method	2.8× increase in drug permeation	125
	Bovine serum albumin (BSA) NPs	HSV	Transcorneal/Ocular	<i>In vitro</i>	173.0 ± 9.5 to 204.7 ± 15.5 nm	0.079 ± 0.023 to 0.226 ± 0.025	—	—	80
	PLGA polymer stabilized with TPGS nanosystem	HSV	Ocular	<i>In vitro, in vivo, ex vivo</i>	262.38 ± 11.85 nm	0.255 ± 0.011	—	58.42 to 80.15% EE <sub>1</sub> %	81
	Carboxymethyl cellulose acetate butyrate NPs	HSV	Intravenous	<i>In vitro</i>	~125–450 nm	—	Precipitation processes (one simple and other rapid)	Drug loading efficiency of 40%	82
	Eudragit RLPO® based NPs	—	Oral	<i>In vitro</i>	82 ± 3.83 nm to 532 ± 4.86 nm	0.308 ± 0.24 to 0.716 ± 0.25	Nanoprecipitation technique	79.34 ± 1.64% EE <sub>2</sub> %	126
	Chitosan NPs	HSV	Topical delivery	<i>In vitro</i>	240.0 ± 62.4 nm	0.53 ± 0.12	Using cross-linked chitosan with tripolyphosphate (TPP)	16% EE <sub>1</sub> %	127
	Chitosan NPs	OVI	Ocular	<i>In vitro</i>	200–495 nm	—	Ionic gelation technique	56 to 80% EE <sub>1</sub> %	128
	Microemulsions (ME)	Herpes virus infections	Topical	<i>In vitro</i>	6.2 ± 0.2 nm to 15.1 ± 1.5 nm	—	Pseudo ternary phase diagrams	2× fold increase in ACV accumulation	129
	β-Cyclodextrin-poly(4-acryloylmorpholine) mono-conjugate (β-CD-PACM)	HSV-1	Oral	<i>In vitro</i>	150 nm (unloaded) and 200 nm when (loaded)	—	Solvent injection technique	83% EE <sub>1</sub> %	130
	Liposomes	HSV	Intranasal	<i>In vivo</i>	1048.1 ± 101.3 nm and 627.4 ± 36.9 nm (for two methods)	—	Drug lipid film hydration method	43.20%	131
Adefovir dipivoxil	Bovine serum albumin (BSA) NPs	HSV	Ocular	<i>In vitro</i>	~200 nm	—	Desolvation method	84.59 ± 1.81 and 52.05 ± 2.03 EE <sub>2</sub> %	132
	SILNs	HBV	—	<i>In vitro</i>	389.4 ± 166.5	-0.371	Solvent diffusion method	15% EE <sub>2</sub> %	133
Atazanavir	Eudragit RL100 NPs (ATV NPs)	HIV	Oral	<i>In vitro, in vivo</i>	465.59 nm	0.372	Nanoprecipitation method	41.3 to 56.9% EE <sub>1</sub> %	134

Table 2 (Contd.)

Antiviral Drug	Nanoparticle(s)	Action against virus	Route of administration	<i>In vitro/in vivo/ex vivo</i>	Size (nm)	Polydispersity index [PDI]	Synthesis method	Efficiency	Reference
Atazanavir and darunavir	LNPs	HIV	Subcutaneous	—	33.6–35.6 nm	—	Sonication of hydrated lipid–drug suspension	85.5 ± 8.2 [ATV], 85.1 ± 7.1 [RTV], and 6.1 ± 0.8% [TFV] EE <sub>2</sub> %	135
Atazanavir, efavirenz, and ritonavir	Atazanavir, efavirenz, and ritonavir NPs (nano ART)	HIV-1	Parenteral administration	—	300–645 nm	—	High-pressure homogenization	—	136
Azidothymidine	Galactosylated liposomes	AIDS6	Intravenous	<i>In vitro</i>	120.01 ± 2.11 nm	—	Esterification of galactose	EE <sub>2</sub> % (L1 to L4): 42.35 ± 0.38, 54.26 ± 3.25, 36.69 ± 3.10, 31.44 ± 2.22 (%)	137
Atazanavir and darunavir	Lipid polymer hybrid NPs (LPHNs)	HIV	Oral	<i>In vitro</i>	50 nm	—	One-step optimized nanoprecipitation method	62, 68.1 and 68.5% w/w EE <sub>1</sub> %	138
Dolutegravir	Chitosan-based polymeric NPs	HIV	Oral	—	140–548 nm	—	3-Step process demineralization, deproteination, and deacetylation	—	139
Dolutegravir sodium	β-Cyclodextrin-based NPs	Neuro-AIDS	Intranasal	<i>In vitro, in vivo</i>	72.47 ± 4.8 to 106.5 ± 5.6 nm	0.306 ± 0.002 and 0.475 ± 0.004	Cross-linking hydroxypropyl β-cyclodextrin (HPβCD) with diphenyl carbonate	77 ± 3.35% EE <sub>2</sub> %	140
Efavirenz	Chitosan NPs	HIV	Oral	<i>In vitro</i>	±104 nm	—	Ionotropic gelation method	91.09% EE <sub>2</sub> %	141
	Eudragit E100	HIV/AIDS	Oral	<i>In vitro, in vivo</i>	110 ± 5 nm	0.201 ± 0.05	Emulsion solvent evaporation method	99% EE <sub>2</sub> %	84
	Lactoferrin NPs	HIV	Oral	<i>In vitro, in vivo</i>	45 ± 60 nm	<0.341	Sol-oil protocol	2 × times improved anti-HIV-1 action compared to free EFV	85
	SLNs	HIV	Oral	<i>In vitro, in vivo</i>	168 nm	<0.220	Hot homogenization technique followed by ultrasonication method	60 ± 5% EE <sub>2</sub> %	142
	SLNs	HIV	Oral	<i>In vitro</i>	124.5 ± 3.2 nm	0.234	—	86% EE <sub>2</sub> %	143
	Poly(epsilon-caprolactone) (PCL) NPs	HIV/AIDS	Oral	<i>In vitro, in vivo</i>	200–250 nm	Narrow	Double-emulsion/spray-drying method	86–93% EE <sub>1</sub> %	144
	Nanoemulsion of EFV	HIV/AIDS	Oral	<i>In vitro, in vivo</i>	Less than 30 nm	—	Phase inversion composition method	80% release within 6 hours	145
	Chitosan-g-HPβCD NPs	Neuro-AIDS	Intranasal	<i>In vitro, in vivo</i>	198 ± 4.4 nm	0.325 ± 0.004 to 0.675 ± 0.005	Ionic gelation method	38 ± 1.43% EE <sub>2</sub> %	145
Efavirenz (EFV) and lopinavir/ritonavir (for boost)	PLGA NPs	HIV	Intracellular	<i>In vitro</i>	138.3–55.4 nm	—	High-pressure homogenization method	>79% EE <sub>2</sub> %	146





Table 2 (Contd.)

Antiviral Drug	Nanoparticle(s)	Action against virus	Route of administration	<i>In vitro/in vivo/ex vivo</i>	Size (nm)	Polydispersity index [PDI]	Synthesis method	Efficiency	Reference
Efavirenz and nevirapine	SLN	HIV/AIDS	—	<i>In vitro</i>	128.7 nm to 182.2 nm	—	Modified emulsion/microemulsion procedure	EFV ~98% and NVP ~30% EE <sub>2</sub> %	147
Elvitegravir	PLGA-EVG NPs	HIV-1	Intraperitoneally	<i>In vitro, in vivo</i>	Less than 200 nm	—	Nano-precipitation technique	~95% loading efficiency of drug	148
Enfuvirtide and protoporphylin IX	PLGA-EVG NPs	HIV-1	—	<i>In vitro</i>	~47 nm	—	Nano-precipitation technique	~92% EE <sub>1</sub> %	149
Foscarnet	Nano-liposome	HIV-1	Intravenous and intramuscular administration	<i>In vitro</i>	—	—	Surfactant-based nanoparticles A rapid extrusion procedure	—	150
Griffithsin (GRFT) (an anti-viral lectin)	Chitosan NPs	HIV-1, herpesvirus DNA polymerase	Oral, topical	<i>In vitro, in vivo</i>	292 ± 5 nm to 497 ± 13 nm	0.26 ± 0.01 to 0.78 ± 0.21	—	—	151
Indinavir	mPEG-PLGA GRFT NPs	HIV-1, HSV-2	Topical	<i>In vitro, in vivo</i>	152 to 345 nm	—	Double emulsion solvent evaporation technique	85.6 ± 11.0 EE <sub>1</sub> %	152
Indinavir	Lipid nanoemulsion (LNE)	HIV	Intravenous	<i>In vitro, in vivo</i>	200.1 ± 73.2 nm (lowest value)	0.05 ± 0.04	—	98.8%, 98.9% and 99.0% EE <sub>2</sub> %	109
Indinavir and lactoferrin	Monoolein-based NPs	HIV	Oral	<i>In vitro</i>	155 ± 7 nm	0.16 ± 0.03	Magnetic stirring and high-pressure homogenization	96% drug incorporation efficiency	108
Ivermectin	mPEG-PCL NPs	HIV	Oral	<i>In vivo</i>	211 ± 10.12 nm (mean particle size)	0.22 to 0.68	Emulsification solvent evaporation method	60%, 40% and 15% drug release percent	107
Lamivudine	Nanoemulsion	HIV	Drug injection	<i>In vitro, in vivo</i>	112 ± 3.5 nm	0.20 ± 0.02	High-speed homogenization method	—	153
Lopinavir	Ivermectin NPs	ZIKV	Oral	<i>In vitro, in vivo</i>	~65 nm	—	—	Conjugation efficiency of ~60% for empty NPs and ~40% for 20% IVM feed loaded NPs	154
Lopinavir	Chitosan NPs	HIV-1	Oral	<i>In vitro, in vivo</i>	120.7 ± 3.1 nm [CS-NPs]; 145.8 ± 4.2 [GL-LMWC-NPs]	0.09 ± 0.01 [CS-NPs]; 0.11 ± 0.06 [GL-LMWC-NPs]	Depolymerization followed by ionotropic gelation method	71.37 ± 1.19% EE <sub>1</sub> %	117
Lopinavir	MLNs	—	Topical (semisolid) or oral (after resuspension)	<i>In vitro</i>	~450 nm	<0.3	Hot homogenization method in conjunction with high shear and ultrasonication	—	118
Lopinavir	SLN	HIV/AIDS	Oral	<i>In vivo</i>	196.5 ± 3.5 nm	0.11 ± 0.01	Warm oil-in-water (O/W) micro-emulsion technique	EE (%) 76.5 ± 3.5%	101
Lopinavir	<i>In situ</i> self-assembly nanoparticles (ISNPs)	HIV	Oral	<i>In vitro, in vivo</i>	Less than 158 nm	—	Warm microemulsion precursors with modification	95% EE <sub>2</sub> %	100



Table 2 (Contd.)

Antiviral Drug	Nanoparticle(s)	Action against virus	Route of administration	<i>In vitro/in vivo/ex vivo</i>	Size (nm)	Polydispersity index [PDI]	Synthesis method	Efficiency	Reference
	PLGA NPs	HIV/AIDS	Oral	<i>In vitro, in vivo</i>	142.1 ± 2.13 nm	—	Solvent diffusion (nanoprecipitation) method	93.03 ± 1.27% EE <sub>2</sub> %	155
	Pullulan acetate NPs	HIV/AIDS	Oral	<i>In vitro, in vivo</i>	197 ± 4 nm (~197 nm)	<0.2	Motozato's method	75% EE <sub>2</sub> %	103
	Poly-ε-caprolactone (PCL) nanoparticles (NPs)	HIV/AIDS	Oral	<i>In vitro, in vivo, ex vivo</i>	195.3 ± 2.3 nm	0.10 ± 0.01	Oil-in-water emulsion-solvent evaporation technique	93.9% EE <sub>2</sub> %	156
	SLNs	HIV/AIDS	Oral	<i>In vitro, in vivo</i>	180.6 ± 2.32 nm	0.133 ± 0.001	Hot self-nano emulsification (SNE) technique	91.5 ± 1.3% EE <sub>2</sub> %	102
	Compritol®-SLNs	HIV/AIDS	Oral	<i>In vivo</i>	156 nm	—	Hot homogenization method followed by ultrasonication	98.99% EE <sub>2</sub> % (highest)	157
Lopinavir–ritonavir–tenofovir	Drug-combination nanoparticles (DcNPs)	HIV	Subcutaneous	<i>In vitro</i>	—	—	Aseptic technique	Highest drug association efficiency of 99 ± 8.2% for lopinavir, 92 ± 7.1% for ritonavir and 10 ± 0.8% for tenofovir	158
Nevirapine	Mesoporous silica nanoparticles (MSNPs)	HIV-1	—	<i>In vitro</i>	60 nm	—	Stober's method	—	159
	PS80-coated PCL NPs	HIV/AIDS	Intravenous	<i>In vitro, in vivo</i>	218.3 ± 7.3 nm	0.283 ± 0.038; 0.179 ± 0.00	Emulsion solvent evaporation technique	50.71% EE <sub>2</sub> % (highest)	160
	Cellulose acetate butyrate (CAB) NPs	HIV/AIDS	—	<i>In vitro</i>	305.76 ± 5.7 nm	0.29 ± 0.03	Emulsification solvent evaporation method	75.89 ± 1.36% EE <sub>1</sub> %	161
	Nanoliposomes	HIV/AIDS	—	<i>In vitro</i>	157 nm	—	Thin-film hydration	78.14% and 76.25% EE <sub>1</sub> %	162
Oseltamivir	SeNPs	EV71	—	<i>In vitro</i>	10 nm	—	—	—	50
Raltegravir + efavirenz	PLGA NPs	HIV	Intravaginal	<i>In vitro</i>	81.8 ± 6.4 nm	—	Emulsion-solvent evaporation method	55.5% [RAL] and 98.2% [EFV] EE <sub>1</sub> %	163
Ritonavir	SLNs	HIV-1	Oral	<i>In vitro</i>	170–250 nm	0.2	Solvent emulsification method and double emulsion method	53.2% EE <sub>2</sub> %	164
	SLNs	HIV/AIDS	Oral	<i>In vitro, in vivo</i>	Less than 300 nm	0.361	Solvent evaporation followed by ultrasonication	53.20 ± 4.13 to 73.04 ± 2.85% EE <sub>1</sub> %	165
	PLGA NPs	HIV/AIDS	—	—	42–102 nm	0.381	Solid-in-oil-in-water (s/o/w) solvent evaporation technique with some changes	75% EE <sub>1</sub> %	166
	Lopinavir (LPN) NPs	HIV-1	Oral	—	~320 nm	<0.2	—	—	167





Table 2 (Contd.)

Antiviral Drug	Nanoparticle(s)	Action against virus	Route of administration	<i>In vitro/in vivo/ex vivo</i>	Size (nm)	Polydispersity index [PDI]	Synthesis method	Efficiency	Reference
Saliphenylhalamide (Saliphe)	SINPs	Influenza A viruses (IAVs)	Inhalation or intravenous (envisioned)	<i>In vitro, in vivo</i>	129 ± 10 nm	0.112	Antisolvent precipitation and high-pressure homogenization techniques	—	168
	SQV NPs	HIV	Oral	<i>In vitro</i>	136–158 nm	—	Interfacial polymer technique	> 97% EE <sub>1</sub> %	105
	SQV nanocrystals	HIV	Oral	<i>In vivo, ex vivo</i>	205.93 ± 3.74 nm	0.1	Anti-solvent precipitation high-pressure homogenization method	—	106
Stavudine	Chitosan NPs	AIDS	—	<i>In vitro</i>	10–200 nm	—	Ionic gelation technique	72% EE <sub>1</sub> %	169
	SINs	HIV/AIDS	Intravenous	—	120 nm to 450 nm	—	—	—	170
	SINs	HIV	Oral	<i>In vitro, in vivo</i>	215 ± 9 nm [SINs]; 344 ± 16 nm [SINs]	0.196 ± 0.019 of SNS	Hot high-pressure homogenization (HPH) method	79.24 ± 1.53% EE <sub>2</sub> %	104
Stavudine, delavirdine, and saquinavir	Chitosan NPs	HIV	Oral	<i>In vitro</i>	212 nm (PSD)	—	Ionic gelation of chitosan with tripolyphosphate anions	85.8 ± 0.16% EE <sub>2</sub> % (highest)	171
	SINs	HIV-1/AIDS	Intravenous	<i>In vitro, in vivo, ex-vivo</i>	75 ± 1.22 nm	0.12	Homogenization	High labeling efficiency	172
	Mannosylated liposomes	HIV	Intravenous	<i>In vitro, in vivo</i>	120 ± 1.52 nm	—	Esterification of mannose	47.2 ± 1.57% EE <sub>2</sub> %	173
Tenofovir	SINs	HIV/AIDS	—	—	142–294 nm	—	Involves emulsion	—	174
	Thiolated chitosan (TCS) core/shell nanofiber (NF)	HIV-1	Topical	<i>In vitro, in vivo</i>	58.81 nm	—	Coaxial electrospinning technique	95% (in 5 hours)	123
	Chitosan NPs (PLGA)/stearylamine (SA) composite NPs	HIV	Vaginal route	<i>In vitro, in vivo, ex vivo</i>	545.1 ± 69.17 nm 127 ± 1 nm	0.663 ± 0.107 0.27 ± 0.01	Ionic gelation Double emulsion/solvent evaporation method	6.8 ± 3.1 EE <sub>1</sub> % Drug association efficiency >50%	121 120
Tenofovir	Chitosan-thioglycolic acid-conjugated (CS-TGA) NPs	HIV/AIDS	Topical	<i>In vitro</i>	240.1 nm CS NPs; 252.3 nm CS-TGA NPs	0.298 ± 0.002 [CS]; 0.317 ± 0.052 [CS-TGA]	Ionotropic gelation	22.60% EE <sub>1</sub> %	122
	PLGA NPs loaded with efavirenz NPs or saquinavir NPs	HIV-1 BaL infection	Topical	<i>In vitro</i>	227 ± 1.8 nm [EFV]; 189 ± 96.3 nm [SQV]	0.05 [EFV]; 0.486 [SQV]	Emulsion or nanoprecipitation techniques	44.5 ± 2.7 [EFV] and 48.3 ± 15.2 [SQV]	175



Table 2 (Contd.)

Antiviral Drug	Nanoparticle(s)	Action against virus	Route of administration	<i>In vitro/in vivo/ex vivo</i>	Size (nm)	Polydispersity index [PDI]	Synthesis method	Efficiency	Reference
Tenofovir, alafenamide and elvitegravir	TAF + EVG NPs	HIV	Subcutaneous	<i>In vitro, in vivo</i>	190.2 ± 2.3 nm	0.14 ± 0.01	Oil-in-water emulsion solvent evaporation technique	54.1 ± 3.6 [TAF] and 44.6 ± 2.4% [EVG] EE <sub>1</sub> %	176
Tenofovir alafenamide	Emtricitabine (FTC) loaded NPs	HIV-1	Subcutaneous and oral	<i>In vivo, ex vivo</i>	233.2 ± 12.8 nm	0.11 ± 0.05	Oil-in-water emulsion solvent evaporation technique	69.2 ± 14.5% [TAF] and 65.9 ± 18.2% [FTC] EE <sub>1</sub> %	177
Tenofovir disoproxil fumarate	Chitosan NPs	HIV/AIDS	Oral	<i>In vitro, in vivo, ex vivo</i>	156 ± 5 nm	0.16 ± 0.06	Ionic gelation technique	48.2 ± 1% EE <sub>2</sub> %	178
Valacyclovir	PLA-PEG NPs	HSV	Oral	<i>In vitro, in vivo</i>	~30 nm	—	Nanoprecipitation	11.4 ± 0.5 EE <sub>2</sub> % (highest)	179
	SILNs	HSV	Ocular	<i>In vitro, in vivo, ex vivo</i>	202.5 ± 2.56 nm	0.252 ± 0.06	Solvent emulsification/evaporation method	28.01 ± 1.89 to 58.82 ± 2.45% EE <sub>2</sub> %	180
Zidovudine	NLCs	HIV	Oral	<i>In vitro</i>	100 to 300 nm	< 0.3	Hot ultrasonication and microwave assisted method	44 ± 3%, 22 ± 2% EE <sub>2</sub> %	181
	Alginate NPs	HIV/AIDS	Intravenous	<i>In vitro</i>	432 ± 11.9 nm	—	Emulsion solvent evaporation method	Loading efficacy of 29.5 ± 3.2%	88
	Lipid NPs modified with polymer gelatin	HIV/AIDS	Oral and topical	<i>In vitro</i>	224 ± 31.2 nm [PLNs of SA]; 291.2 ± 38 nm [PLNs of comp]	—	—	87.4 ± 0.58% EE <sub>1</sub> %	89
	Nanosized polyelectrolyte complexes (PECs)	HIV	—	<i>In vitro</i>	100–200 nm	0.125–0.305	—	Drug release of 38.1% at pH 4.5 and 31.2% at pH 7.4	182
	SILNs	HIV	Parenteral, oral, ophthalmic, and topical	—	222–227 nm [AZT-SA], 402 nm to 434 nm [AZT-SA-AV]	0.2 to 0.3 [AZA-SA], 0.38–0.45 [AZT-SA-AV]	Simple emulsion solvent evaporation method	74.92 ± 1.2% EE <sub>1</sub> %	92
	Chitosan NPs	AIDS	Nasal	—	260 ± 1.70 nm, 330 ± 12.9 [NP1, NP2]; 406 ± 14.0 and 425 ± 14.5 for AZT-loaded NP1 and NP2	0.247, 0.329, 0.390, 0.381	Ionotropic gelation method	17.58% ± 1.48 and 11.02% ± 2.05 EE <sub>2</sub> % for NP <sub>1</sub> and NP <sub>2</sub>	183
	Lipid-polymer hybrid NP	HIV	—	<i>In vitro</i>	175 ± 2.5 nm	0.196	Melt emulsification-probe sonication technique	6.5 ± 0.50 to 49.26 ± 0.75% EE <sub>2</sub> %	184
	PLA-PEG blend NPs	AIDS	Intranasal	<i>In vivo</i>	328.1 ± 8.6 nm	0.383	Double emulsion- evaporation method	52% EE <sub>1</sub> %	185
	SILNs	AIDS	Oral	<i>In vitro</i>	621 nm	—	W/o/w double-emulsion solvent-evaporation method	27% EE <sub>2</sub> %	186
	Dextran and stearic acid NPs	HIV/AIDS	Intravenous	<i>In vitro, in vivo</i>	356 nm to 730 nm	—	Double emulsion solvent evaporation method	93.46% EE <sub>1</sub> %	86

Table 2 (Contd.)

Antiviral Drug	Nanoparticle(s)	Action against virus	Route of administration	<i>In vitro/in vivo/ex vivo</i>	Size (nm)	Polydispersity index [PDI]	Synthesis method	Efficiency	Reference
	PVP/SA-PEG NPs (PSNPs)	AIDS	Intravenous	<i>In vitro</i>	341 ± 4.34 nm	0.3 ± 0.04	Emulsification-solvent evaporation method	37.19% to 79.2%	87
	Hybrid NPs of CMC-AZT core enclosed by shell of Comp-PEG	AIDS	Oral	<i>In vitro</i>	161.65 ± 44.06 nm	—	—	82% EE <sub>1</sub> %	90
Zidovudine + efavirenz + lamivudine	Lactoferrin NPs	HIV	Oral	<i>In vitro, in vivo</i>	67 nm	—	Sol-oil protocol	58 to 71% EE <sub>1</sub> %	187

and the film which essentially implies uniform distribution of particles. The thicknesses of NPs-in-film and the film were in general agreement with values 85 μm and 70 μm, respectively. Possible reason for this difference can be the presence of vacuum inside the SEM chamber which may have caused the film to retract. Further observations with SEM show surfaces of NP-in-film and the film were quite homogeneous with the exception to presence of some scales on the TFV-film (Fig. 13a(C and D)). The cause of precipitation can be the incomplete solubilization of free TFV during the drying process. Similarly, absence of scales for TFV-PLGA/SA NPs-in-film indicates effective solubilization thanks to incorporated particles. The elemental analysis results did not indicate the presence of phosphorous which is present in the phosphonate group of TFV (Fig. 13a(E)). This means that drug was so deeply embedded in the film that even incident electron beam was not able to detect it. Presence of TFV was detected on the TFV film by the same EDS analysis as seen in Fig. 13a(F). The release profiles were recorded for NPs-in-film, TFV film alone and for prepared NPs and they are shown in Fig. 13b. TFV film exhibited initial burst release by releasing about 80% of its drug in the first few minutes and then after 2 hours about 90% drug was released. This result was obvious as TFV is a highly water-soluble drug and has a quick disintegration time. Secondly, the films containing TFV-loaded NPs showed mild burst release at first by releasing about 30% of the drug in 15 minutes, followed by a controlled release. Total drug released after 24 h was nearly 60%. The release was initially rapid as TFV was present at the surface of NPs as observed also for TFV film (NPs not incorporated). The release profile for TFV-PLGA-SA NPs not incorporated in film is like that of NPs-in-film. However, the film matrix imposed a delaying effect on the release of TFV during film disaggregation for 24 h. This effect was enhanced by the presence of PVA/HPMC on the surface of NPs, providing further hindrance to drug release. This biphasic release pattern is beneficial in the sense that initial burst release creates high genital levels of TFV which provide immediate protection while assuring sustained release for many hours. To evaluate the *in vivo* safety of the prepared films regarding possible toxicity which may arise later, a 14 days study was conducted. Both TFV-film and NPs-in-film were subjected to daily vaginal administration. Mice given PBS washing or vaginally administered with Film or VCF® were taken as controls. No biological change which could indicate the toxic nature of films was recorded during the study as vaginal administration to mice did not show any adverse effect on health, size, or weight. Vaginal histology of mice showed change only in the case of VCF®, as seen in Fig. 13c. This mild thinning of epithelium was verified by assessment of an average number of epithelial cell layers as shown in Fig. 13d. The mouse model was used for the first time to determine the safety of vaginal films and they were found to be biologically safe to be administered to women (Fig. 13e). The vaginal films can also be a temporary substitute for rings for women requiring occasional protection as they showed quick disintegration once in contact with the simulated vaginal fluid (SVF).



Another study examined a thermogelling system containing TFV-loaded with chitosan NPs synthesized *via* ionic gelation method.<sup>121</sup> The biocompatible formulation reached a size of  $545.1 \pm 69.17$  nm once the drug was incorporated into NPs. Gelation temperature of the gel was tolerable for the administration to women and the gelation starts once it is fully administered to the vagina. However, due to the high water solubility of TFV, the NPs showed very low encapsulation efficiency ( $6.8 \pm 3.1\%$ ) and drug loading content of  $1.86 \pm 0.85\%$ . The *in vitro* study showed that the initial burst release effect was reduced to 27% with the formulation. The prepared vaginal gel holds significance in ease of administration as well as effectiveness for the treatment of women suffering from HIV.

Meng *et al.* examined the effects of TFV loaded with CS-TGA NPs against HIV prevention.<sup>122</sup> They used ionotropic gelation to prepare CS-TGA NPs of mean size between 240–252 nm. Greater encapsulation efficiency of 22.60% was recorded than the study quoted previously. Both NPs did not show any toxicity in 2 days. The percentage of mucoadhesion was five times greater in CS-TGA NPs than CS-NPs. This shows that the prepared NPs have the potential to increase the retention time of TFV, hence making it more effective in the treatment of HIV.

Thiolated chitosan (TCS) core/shell nanofiber (NF) can improve the loading capacity of TFV.<sup>123</sup> As stated previously, TFV is highly water-soluble. The coaxial electrospinning technique was utilized to prepare NFs having a core of PEO and shell composed of PLA/TCS. The NFs reached a mean diameter of 99.53 nm with smooth surface morphology. They were found to be safe for topical administration. A significant increase in drug loading capacity was recorded. At concentration of  $1 \text{ mg mL}^{-1}$ , NFs were non-cytotoxic. Their biocompatibility was proved from *in vivo* studies. Hence TCS core/shell NFs can be employed as a delivery vehicle of TFV. Table 2 presents a summary of various studies over the past decade showing well known antiviral drugs and their combinations with NPs along with other important parameters.

## 4. Conclusion

The established potential of nanotechnology in antiviral applications coupled with massive progress in designing wide categories of different nanomaterials-based antiviral drugs gives many expectations to the research community to explore their potential further to overcome their existing drawbacks. The nano-based systems can prove fruitful in overcoming the associated drawbacks with the current therapies such as low oral bioavailability, issues with hemocompatibility, chances for skin diseases due to topical exposure of drug, toxic nature of the drug, reduction in drug's effectiveness due to frequent administration, to name a few. However, as per the best of our knowledge, most of these nano-based systems designed to date are not approved for clinical use or are still under clinical trials, despite exhaustive and continued effort for more than 24 years. It is expected that in upcoming years, we shall witness more clinical approvals and applications of these nano-based systems which will definitely help overcome the health issues globally.

## 5. Future perspectives

Tuning at the nanoscale can give us interesting properties for a range of applications. In our review, we have covered many functional metallic NPs as well as a variety of drugs that can be tailored by using NPs as their delivery vehicles. However, in order to treat patients globally in vast numbers (such as with COVID-19 pandemic recently), it is not possible to develop antiviral drugs in such a short span of time and fully overcome their existing drawbacks. As we discussed earlier, frequent drug administration is itself counterproductive since it generates an immune response from body and increases its drug resistance resulting in a decline in the drug's efficiency. Moreover, the route of administration for each drug must be carefully chosen. There are associated disadvantages with the choice of each route. For instance, oral administration may not be feasible for children, ocular delivery could prove detrimental for eyes and topical exposure of drug to skin may cause skin diseases. On contrary, vaccines have proven to be a rather better option in fighting pandemics in the past century. However, vaccines also have associated shortcomings such as insufficient cellular immunity, risk of antibodies dependent enhancements (ADE) and lack of cross-permeation. Our discussion regarding the potential of nanomaterials in antiviral applications gives useful insight that they can be a good candidate in development of novel vaccines against various viral infections. We suggest the scientific community and interested researchers to also focus on further development of these “nanovaccines”, evaluate their potential against viruses, weigh their pros and cons, and explore methods for their cost-effective and large-scale manufacturing so that they can deal with current and upcoming global health challenges posed by such highly unpredictable viral outbreaks.

## Author contributions

Muhammad Aanish Ali (drafting and paper writing); Dr Nagina Rehman (drafting and reviewing the paper); Dr Tae Joo Park (resources and supervision); Dr Muhammad Abdul Basit (conceptualization, resources and data analysis).

## Conflicts of interest

The authors declare that they have no known competing financial interests or personal relationships that could have appeared to influence the work reported in this paper.

## Acknowledgements

The work is mainly done at Department of Materials Science and Engineering at Institute of Space Technology, Pakistan and supported by NEL, Hanyang University South Korea from Project No. 20010727 (Technology Innovation Program by Ministry of Trade, Industry and Energy Korea).





## References

- 1 R. E. Kahn, W. Ma and J. A. Richt, in *Influenza Pathogenesis and Control - Volume I*, ed. R. W. Compans and M. B. A. Oldstone, Springer International Publishing, Cham, 2014, pp. 205–218.
- 2 M. Qasim, D.-J. Lim, H. Park and D. Na, *J. Nanosci. Nanotechnol.*, 2014, **14**, 7374–7387.
- 3 C. Wejse, C. B. Patsche, A. Kühle, F. J. V. Bamba, M. S. Mendes, G. Lemvik, V. F. Gomes and F. Rudolf, *Int. J. Infect. Dis.*, 2015, **32**, 128–134.
- 4 C. R. Braden, S. F. Dowell, D. B. Jernigan and J. M. Hughes, *Emerging Infect. Dis.*, 2013, **19**, 864–869.
- 5 M. Breitbart and F. Rohwer, *Trends Microbiol.*, 2005, **13**, 278–284.
- 6 L. Chen and J. Liang, *Mater. Sci. Eng. C*, 2020, **112**, 110924.
- 7 A. Rivera and I. Messaoudi, *ACS Infectious Diseases*, 2015, **1**, 186–197.
- 8 C. J. Schweitzer and T. J. Liang, *ACS Infectious Diseases*, 2016, **1**, 416–419.
- 9 B. A. Aderibigbe, *Molecules*, 2017, **22**, 1370.
- 10 S. Galdiero, A. Falanga, M. Vitiello, M. Cantisani, V. Marra and M. Galdiero, *Molecules*, 2011, **16**, 8894–8918.
- 11 D. M. Coen and R. J. Whitley, *Curr. Opin. Virol.*, 2011, **1**, 545–547.
- 12 F. Corsi, L. Sorrentino, S. Mazzucchelli, M. Truffi, A. Capetti, G. Rizzardini and L. Fiandra, *J. Pharm. Pharmacol.*, 2016, **4**, 328–339.
- 13 D. Lembo, M. Donalisio, A. Civra, M. Argenziano and R. Cavalli, *Expert Opin. Drug Delivery*, 2018, **15**, 93–114.
- 14 L. Calderón, R. Harris, M. Cordoba-Diaz, M. Elorza, B. Elorza, J. Lenoir, E. Adriaens, J. P. Remon, A. Heras and D. Cordoba-Diaz, *Eur. J. Pharm. Sci.*, 2013, **48**, 216–222.
- 15 T. Q. Huy, N. T. Hien Thanh, N. T. Thuy, P. Van Chung, P. N. Hung, A. T. Le and N. T. Hong Hanh, *J. Virol. Methods*, 2017, **241**, 52–57.
- 16 D. Morris, M. Ansar, J. Speshock, T. Ivanciuc, Y. Qu, A. Casola and R. Garofalo, *Viruses*, 2019, **11**, 732.
- 17 Y. Li, Z. Lin, T. Xu, C. Wang, M. Zhao, M. Xiao, H. Wang, N. Deng and B. Zhu, *RSC Adv.*, 2017, **7**, 1453–1463.
- 18 T. Q. Huy, N. T. Hien Thanh, N. T. Thuy, P. Van Chung, P. N. Hung, A. T. Le and N. T. Hong Hanh, *J. Virol. Methods*, 2017, **241**, 52–57.
- 19 E. Szymańska, P. Orłowski, K. Winnicka, E. Tomaszewska, P. Baska, G. Celichowski, J. Grobelny, A. Basa and M. Krzyżowska, *Int. J. Mol. Sci.*, 2018, **19**, 387.
- 20 M. M. El-Sheekh, M. T. Shabaan, L. Hassan and H. H. Morsi, *Int. J. Environ. Health Res.*, 2020, 1–12.
- 21 E. G. Haggag, A. M. Elshamy, M. A. Rabeh, N. M. Gabr, M. Salem, K. A. Youssif, A. Samir, A. Bin Muhsinah, A. Alsayari and U. R. Abdelmohsen, *Int. J. Nanomed.*, 2019, **14**, 6217–6229.
- 22 T. V. M. Sreekanth, P. C. Nagajyothi, P. Muthuraman, G. Enkhtaivan, S. V. P. Vattikuti, C. O. Tettey, D. H. Kim, J. Shim and K. Yoo, *J. Photochem. Photobiol., B*, 2018, **188**, 6–11.
- 23 D. xi Xiang, Q. Chen, L. Pang and C. long Zheng, *J. Virol. Methods*, 2011, **178**, 137–142.
- 24 D. Xiang, Y. Zheng, W. Duan, X. Li, J. Yin, S. Shigdar, M. L. O'Connor, M. Marappan, X. Zhao, Y. Miao, B. Xiang and C. Zheng, *Int. J. Nanomed.*, 2013, **8**, 4103–4114.
- 25 B. Gerhardson, *Trends Biotechnol.*, 2002, **20**, 338–343.
- 26 A. S. Hamed Derbalah and M. M. Elsharkawy, *J. Biotechnol.*, 2019, **306**, 134–141.
- 27 C. Huo, J. Xiao, K. Xiao, S. Zou, M. Wang, P. Qi, T. Liu and Y. Hu, *Int. J. Nanomed.*, 2020, **15**, 661–674.
- 28 J. N. Makau, K. Watanabe, M. M. D. Mohammed and N. Nishida, *J. Med. Food*, 2018, **21**, 777–784.
- 29 K. S. Siddiqi, A. ur Rahman, Tajuddin and A. Husen, *Nanoscale Res. Lett.*, 2018, **13**(1), 1–13.
- 30 H. Ghaffari, A. Tavakoli, A. Moradi, A. Tabarraei, F. Bokharaei-Salim, M. Zahmatkeshan, M. Farahmand, D. Javanmard, S. J. Kiani, M. Esghaei, V. Pirhajati-Mahabadi, A. Ataei-Pirkooch and S. H. Monavari, *J. Biomed. Sci.*, 2019, **26**, 1–10.
- 31 K. W. BAILISS and S. Senananyake, *Plant Pathol.*, 1984, **33**, 185–192.
- 32 Y. H. Hsueh, K. S. Lin, W. J. Ke, C. Te Hsieh, C. L. Chiang, D. Y. Tzou and S. T. Liu, *PLoS One*, 2015, **10**, e0144306.
- 33 C. Adán, J. Marugán, E. Sánchez, C. Pablos and R. Van Grieken, *Electrochim. Acta*, 2016, **191**, 521–529.
- 34 R. M. Di Piero, Q. S. de Novaes and S. F. Pascholati, *Braz. Arch. Biol. Technol.*, 2010, **53**, 269–278.
- 35 M. M. Elsharkawy and A. Derbalah, *Pest Manage. Sci.*, 2019, **75**, 828–834.
- 36 H. Gomaa, H. Khalifa, M. M. Selim, M. A. Shenashen, S. Kawada, A. S. Alamoudi, A. M. Azzam, A. A. Alhamid and S. A. El-Safty, *ACS Sustainable Chem. Eng.*, 2017, **5**, 10826–10839.
- 37 C. Jia, P. Yang, H. S. Chen and J. Wang, *CrystEngComm*, 2015, **17**, 2940–2948.
- 38 R. Nakano, H. Ishiguro, Y. Yao, J. Kajioaka, A. Fujishima, K. Sunada, M. Minoshima, K. Hashimoto and Y. Kubota, *Photochem. Photobiol. Sci.*, 2012, **11**, 1293–1298.
- 39 Y. N. Chen, Y. H. Hsueh, C. Te Hsieh, D. Y. Tzou and P. L. Chang, *Int. J. Environ. Res. Public Health*, 2016, **13**, 4–6.
- 40 A. Halder, S. Das, D. Ojha, D. Chattopadhyay and A. Mukherjee, *Mater. Sci. Eng. C*, 2018, **89**, 413–421.
- 41 P. Di Gianvincenzo, M. Marradi, O. M. Martínez-Ávila, L. M. Bedoya, J. Alcamí and S. Penadés, *Bioorg. Med. Chem. Lett.*, 2010, **20**, 2718–2721.
- 42 I. Papp, C. Sieben, K. Ludwig, M. Roskamp, C. Böttcher, S. Schlecht, A. Herrmann and R. Haag, *Small*, 2010, **6**, 2900–2906.
- 43 A. M. Paul, Y. Shi, D. Acharya, J. R. Douglas, A. Cooley, J. F. Anderson, F. Huang and F. Bai, *J. Gen. Virol.*, 2014, **95**, 1712–1722.
- 44 Y. Li, Z. Lin, M. Guo, Y. Xia, M. Zhao, C. Wang, T. Xu, T. Chen and B. Zhu, *Int. J. Nanomed.*, 2017, **12**, 5733–5743.
- 45 Z. Lin, Y. Li, G. Gong, Y. Xia, C. Wang, Y. Chen, L. Hua, J. Zhong, Y. Tang, X. Liu and B. Zhu, *Int. J. Nanomed.*, 2018, **13**, 5787–5797.



- 46 Y. Li, T. Xu, Z. Lin, C. Wang, Y. Xia, M. Guo, M. Zhao, Y. Chen and B. Zhu, *ACS Omega*, 2019, **4**, 6720–6725.
- 47 Y. Li, Z. Lin, M. Guo, M. Zhao, Y. Xia, C. Wang, T. Xu and B. Zhu, *Int. J. Nanomed.*, 2018, **13**, 2005–2016.
- 48 A. EA and P. EB, *Int. J. Med. Inform.*, 2019, **125**, 30–36.
- 49 Z. Cheng, X. Zhi, G. Sun, W. Guo, Y. Huang, W. Sun, X. Tian, F. Zhao and K. Hu, *J. Med. Virol.*, 2016, **88**, 653–663.
- 50 J. Zhong, Y. Xia, L. Hua, X. Liu, M. Xiao, T. Xu, B. Zhu and H. Cao, *Artif. Cells, Nanomed., Biotechnol.*, 2019, **47**, 3485–3491.
- 51 T. Du, J. Liang, N. Dong, J. Lu, Y. Fu, L. Fang, S. Xiao and H. Han, *ACS Appl. Mater. Interfaces*, 2018, **10**, 4369–4378.
- 52 V. Sujitha, K. Murugan, M. Paulpandi, C. Panneerselvam, U. Suresh, M. Roni, M. Nicoletti, A. Higuchi, P. Madhiyazhagan, J. Subramaniam, D. Dinesh, C. Vadivalagan, B. Chandramohan, A. A. Alarfaj, M. A. Munusamy, D. R. Barnard and G. Benelli, *Parasitol. Res.*, 2015, **114**, 3315–3325.
- 53 J. Jampilek and K. Král'ová, in *Nanotheranostics: Applications and Limitations*, Nature Publishing Group, 2019, pp. 137–178.
- 54 D. Baram-Pinto, S. Shukla, A. Gedanken and R. Sarid, *Small*, 2010, **6**, 1044–1050.
- 55 M. Z. Fahmi, W. Sukmayani, S. Q. Khairunisa, A. M. Witaningrum, D. W. Indriati, M. Q. Y. Matondang, J. Y. Chang, T. Kotaki and M. Kameoka, *RSC Adv.*, 2016, **6**, 92996–93002.
- 56 A. Łoczechin, K. Séron, A. Barras, E. Giovanelli, S. Belouzard, Y. T. Chen, N. Metzler-Nolte, R. Boukherroub, J. Dubuisson and S. Szunerits, *ACS Appl. Mater. Interfaces*, 2019, **11**, 42964–42974.
- 57 Y. Fujimori, T. Sato, T. Hayata, T. Nagao, M. Nakayama, T. Nakayama, R. Sugamat and K. Suzuki, *Appl. Environ. Microbiol.*, 2012, **78**, 951–955.
- 58 N. Shionoiri, T. Sato, Y. Fujimori, T. Nakayama, M. Nemoto, T. Matsunaga and T. Tanaka, *J. Biosci. Bioeng.*, 2012, **113**, 580–586.
- 59 I. Das Jana, P. Kumbhakar, S. Banerjee, C. C. Gowda, N. Kedia, S. K. Kuila, S. Banerjee, N. C. Das, A. K. Das, I. Manna, C. S. Tiwary and A. Mondal, *ACS Appl. Nano Mater.*, 2021, **4**, 352–362.
- 60 A. Tavakoli and M. S. Hashemzadeh, *J. Virol. Methods*, 2020, **275**, 113688.
- 61 X. Hang, H. Peng, H. Song, Z. Qi, X. Miao and W. Xu, *J. Virol. Methods*, 2015, **222**, 150–157.
- 62 L. Tang, Y. Jiang, M. Zhu, L. Chen, X. Zhou, C. Zhou, P. Ye, X. Chen, B. Wang, Z. Xu, Q. Zhang, X. Xu, H. Gao, X. Wu, D. Li, W. Jiang, J. Qu, C. Xiang and L. Li, *Front. Med.*, 2020, **14**, 664–673.
- 63 R. Kumar, M. Nayak, G. C. Sahoo, K. Pandey, M. C. Sarkar, Y. Ansari, V. N. R. Das, R. K. Topno, Bhawna, M. Madhukar and P. Das, *J. Infect. Chemother.*, 2019, **25**, 325–329.
- 64 Z. Lin, Y. Li, T. Xu, M. Guo, C. Wang, M. Zhao, H. Chen, J. Kuang, W. Li, Y. Zhang, T. Lin, Y. Chen, H. Chen and B. Zhu, *ACS Omega*, 2020, **5**, 12495–12500.
- 65 C. Balagna, S. Perero, E. Percivalle, E. V. Nepita and M. Ferraris, *Open Ceram.*, 2020, **1**, 100006.
- 66 T. Du, J. Lu, L. Liu, N. Dong, L. Fang, S. Xiao and H. Han, *ACS Appl. Bio Mater.*, 2018, **1**, 1286–1293.
- 67 N. A. Mazurkova, Y. E. Spitsyna, N. V. Shikina, Z. R. Ismagilov, S. N. Zagrebel'nyi and E. I. Ryabchikova, *Nanotechnol. Russ.*, 2010, **5**, 417–420.
- 68 F. Pfaff, B. Glück, T. Hoyer, D. Rohländer, A. Sauerbrei and R. Zell, *Lett. Appl. Microbiol.*, 2019, **69**, 302–309.
- 69 S. Mahmood, K. C. Kiong, C. S. Tham, T. C. Chien, A. R. Hilles and J. R. Venugopal, *AAPS PharmSciTech*, 2020, **21**, 1–15.
- 70 S. Ilk, N. Saglam and M. Özgen, *Artif. Cells, Nanomed., Biotechnol.*, 2017, **45**, 907–916.
- 71 S. Raut, S. S. Bhadoriya, V. Uplanchiwar, V. Mishra, A. Gahane and S. K. Jain, *Acta Pharm. Sin. B*, 2012, **2**, 8–15.
- 72 Q. Tan, W. Liu, C. Guo and G. Zhai, *Int. J. Nanomed.*, 2011, **6**, 1621.
- 73 J. J. F. Verhoef and T. J. Anchordoquy, *Drug Delivery Transl. Res.*, 2013, **3**, 499–503.
- 74 S. Mahmood, K. C. Kiong, C. S. Tham, T. C. Chien, A. R. Hilles and J. R. Venugopal, *AAPS PharmSciTech*, 2020, **21**(7), 1–15.
- 75 Z. Saifi, M. Rizwanullah, S. R. Mir and S. Amin, *J. Drug Delivery Sci. Technol.*, 2020, **57**, 101634.
- 76 J. F. Fanguero, T. Andreani, L. Fernandes, M. L. Garcia, M. A. Egea, A. M. Silva and E. B. Souto, *Colloids Surf., B*, 2014, **123**, 452–460.
- 77 K. Cholkar, S. P. Patel, A. D. Vadlapudi and A. K. Mitra, *J. Ocul. Pharmacol. Ther.*, 2013, **29**, 106–123.
- 78 M. H. Warsi, M. Anwar, V. Garg, G. K. Jain, S. Talegaonkar, F. J. Ahmad and R. K. Khar, *Colloids Surf., B*, 2014, **122**, 423–431.
- 79 U. V. Bhosale, V. Kusum Devi and N. Jain, *J. Young Pharm.*, 2011, **3**, 275–283.
- 80 P. Suwannoi, M. Chomnawang, A. Tunsirikongkon, A. Phongphisutthinan, C. C. Müller-Goymann and N. Sarisuta, *J. Drug Delivery Sci. Technol.*, 2019, **52**, 624–631.
- 81 M. Alkholief, H. Albasit, A. Alhowyan, S. Alshehri, M. Raish, M. Abul Kalam and A. Alshamsan, *Saudi Pharm. J.*, 2019, **27**, 293–302.
- 82 V. B. Vedula, M. Chopra, E. Joseph and S. Mazumder, *Appl. Nanosci.*, 2016, **6**, 197–208.
- 83 A. Belgamwar, S. Khan and P. Yeole, *Artif. Cells, Nanomed., Biotechnol.*, 2018, **46**, 374–386.
- 84 B. N. V. Hari, N. Narayanan, K. Dhevendaran and D. Ramyadevi, *Mater. Sci. Eng. C*, 2016, **67**, 522–532.
- 85 P. Kumar, Y. S. Lakshmi and A. K. Kondapi, *HIV Med.*, 2017, **18**, 452–462.
- 86 K. S. Joshy, A. George, S. Snigdha, B. Joseph, N. Kalarikkal, L. A. Pothan and S. Thomas, *Mater. Sci. Eng. C*, 2018, **93**, 864–872.
- 87 K. S. Joshy, S. Snigdha, G. Anne, K. Nandakumar, A. P. Laly and T. Sabu, *Chem. Phys. Lipids*, 2018, **210**, 82–89.
- 88 K. S. Joshy, M. A. Susan, S. Snigdha, K. Nandakumar, A. P. Laly and T. Sabu, *Int. J. Biol. Macromol.*, 2018, **107**, 929–937.
- 89 K. S. Joshy, S. Snigdha, N. Kalarikkal, L. A. Pothan and S. Thomas, *Chem. Phys. Lipids*, 2017, **207**, 24–37.



- 90 K. S. Joshy, S. Snigdha, A. George, N. Kalarikkal, L. A. Pothan and S. Thomas, *Cellulose*, 2017, **24**, 4759–4771.
- 91 A. L. M. Carvalho, J. A. da Silva, A. A. M. Lira, T. M. F. Conceição, R. de S. Nunes, R. L. C. de Albuquerque Junior, V. H. V. Sarmento, L. B. Leal and D. P. de Santana, *J. Pharm. Sci.*, 2016, **105**, 2188–2193.
- 92 K. S. Joshy, C. P. Sharma, N. Kalarikkal, K. Sandeep, S. Thomas and L. A. Pothan, *Mater. Sci. Eng. C*, 2016, **66**, 40–50.
- 93 A. Laux, C. Gouws and J. H. Hamman, *Expert Opin. Drug Delivery*, 2019, **16**, 1283–1285.
- 94 I. Gomez-Orellana, *Expert Opin. Drug Delivery*, 2005, **2**, 419–433.
- 95 S. I. Pather, M. J. Rathbone and S. Senel, *Expert Opin. Drug Delivery*, 2008, **5**, 531–542.
- 96 M. R. Prausnitz and R. Langer, *Nat. Biotechnol.*, 2008, **26**, 1261–1268.
- 97 T. B. Ernest, D. P. Elder, L. G. Martini, M. Roberts and J. L. Ford, *J. Pharm. Pharmacol.*, 2010, **59**, 1043–1055.
- 98 A. Cram, J. Breitzkreutz, S. Desset-Brèthes, T. Nunn and C. Tuleu, *Int. J. Pharm.*, 2009, **365**, 1–3.
- 99 P. N.-W. D. Information and U. 2012, WHO Drug Information International Regulatory Harmonization.
- 100 K. Pham, D. Li, S. Guo, S. Penzak and X. Dong, *J. Controlled Release*, 2016, **226**, 88–97.
- 101 P. R. Ravi and R. Vats, *J. Pharm. Pharmacol.*, 2017, **69**, 823–833.
- 102 J. S. Negi, P. Chattopadhyay, A. K. Sharma and V. Ram, *Eur. J. Pharm. Sci.*, 2013, **48**, 231–239.
- 103 P. R. Ravi, R. Vats, J. Balija, S. P. N. Adapa and N. Aditya, *Carbohydr. Polym.*, 2014, **110**, 320–328.
- 104 S. S. Dodiya, S. S. Chavhan, K. K. Sawant and A. G. Korde, *J. Microencapsulation*, 2011, **28**, 515–527.
- 105 K. Krieser, J. Emanuelli, R. M. Daudt, S. Bilatto, J. B. Willig, S. S. Guterres, A. R. Pohlmann, A. Buffon, D. S. Correa and I. C. Küllkamp-Guerreiro, *Mater. Sci. Eng. C*, 2020, **117**, 111315.
- 106 Y. He, D. N. Xia, Q. X. Li, J. S. Tao, Y. Gan and C. Wang, *Acta Pharmacol. Sin.*, 2015, **36**, 1151–1160.
- 107 M. Kurd, S. S. Malvajerd, S. Rezaee, M. Hamidi and K. Derakhshandeh, *Artif. Cells, Nanomed., Biotechnol.*, 2019, **47**, 2123–2133.
- 108 M. D. Bianchin, G. Prebianca, M. F. Immich, M. L. Teixeira, M. Colombo, L. S. Koester, B. V. de Araújo, F. Poletto and I. C. Küllkamp-Guerreiro, *Drug Dev. Ind. Pharm.*, 2021, **47**, 83–91.
- 109 K. Prabhakar, S. M. Afzal, G. Surender and V. Kishan, *Acta Pharm. Sin. B*, 2013, **3**, 345–353.
- 110 R. Pompei, O. Flore, M. A. Marccialis, A. Pani and B. Loddo, *Nature*, 1979, **281**, 689–690.
- 111 J. Cinatl, B. Morgenstern, G. Bauer, P. Chandra, H. Rabenau and H. W. Doerr, *Lancet*, 2003, **361**, 2045–2046.
- 112 J. L. Chew, C. B. Wolfowicz, H. Q. Mao, K. W. Leong and K. Y. Chua, *Vaccine*, 2003, **21**, 2720–2729.
- 113 Y. Wu, W. Yang, C. Wang, J. Hu and S. Fu, *Int. J. Pharm.*, 2005, **295**, 235–245.
- 114 D. Depan, B. Girase, J. S. Shah and R. D. K. Misra, *Acta Biomater.*, 2011, **7**, 3432–3445.
- 115 D. Depan, P. K. C. Venkata Surya, B. Girase and R. D. K. Misra, *Acta Biomater.*, 2011, **7**, 2163–2175.
- 116 Q. Yuan, S. Hein and R. D. K. Misra, *Acta Biomater.*, 2010, **6**, 2732–2739.
- 117 D. Mishra, N. Jain, V. Rajoriya and A. K. Jain, *J. Pharm. Pharmacol.*, 2014, **66**, 1082–1093.
- 118 S. M. T. Cavalcanti, C. Nunes, S. A. C. Lima, J. L. Soares-Sobrinho and S. Reis, *Pharm. Res.*, 2017, **34**, 1204–1216.
- 119 C. Woodsong and J. D. S. Holt, *Adv. Drug Delivery Rev.*, 2015, **92**, 146–154.
- 120 A. Machado, C. Cunha-Reis, F. Araújo, R. Nunes, V. Seabra, D. Ferreira, J. das Neves and B. Sarmento, *Acta Biomater.*, 2016, **44**, 332–340.
- 121 S. S. Timur, A. Şahin, E. Aytekin, N. Öztürk, K. H. Polat, N. Tezel, R. N. Gürsoy and S. Çaliş, *Pharm. Dev. Technol.*, 2018, **23**, 301–310.
- 122 J. Meng, T. Zhang, V. Agrahari, M. J. Ezoulin and B. B. C. Youan, *Nanomedicine*, 2014, **9**, 1595–1612.
- 123 J. Meng, V. Agrahari, M. J. Ezoulin, C. Zhang, S. S. Purohit, A. Molteni, D. Dim, N. A. Oyler and B. B. C. Youan, *Mol. Pharm.*, 2016, **13**, 4129–4140.
- 124 R. Parthiban, Shanmugapriya, Indhu, Sathishkumar, Surendhar and R. Prakash, *Drug Invent. Today*, 2020, **14**, 108–111.
- 125 M. M. Mahboobian, M. Mohammadi and Z. Mansouri, *J. Drug Delivery Sci. Technol.*, 2020, **55**, 101400.
- 126 A. Gandhi, S. Jana and K. K. Sen, *Int. J. Biol. Macromol.*, 2014, **67**, 478–482.
- 127 L. Calderón, R. Harris, M. Cordoba-Diaz, M. Elorza, B. Elorza, J. Lenoir, E. Adriaens, J. P. Remon, A. Heras and D. Cordoba-Diaz, *Eur. J. Pharm. Sci.*, 2013, **48**, 216–222.
- 128 N. Rajendran, R. Natrajan, R. Kumar and S. Selvaraj, *Asian J. Pharm.*, 2010, **4**, 220–226.
- 129 E. Peira, D. Chirio, M. E. Carlotti, R. Spagnolo and M. Trotta, *J. Drug Delivery Sci. Technol.*, 2009, **19**, 191–196.
- 130 R. Cavalli, M. Donalisio, A. Civra, P. Ferruti, E. Ranucci, F. Trotta and D. Lembo, *J. Controlled Release*, 2009, **137**, 116–122.
- 131 I. A. Alsarra, A. Y. Hamed and F. K. Alanazi, *Drug Delivery*, 2008, **15**, 313–321.
- 132 P. Suwannoi, M. Chomnawang, N. Sarisuta, S. Reichl and C. C. Müller-Goymann, *J. Ocul. Pharmacol. Ther.*, 2017, **33**, 743–752.
- 133 Z. Xing-Guo, M. Jing, L. Min-Wei, J. Sai-Ping, H. Fu-Qiang and D. Yong-Zhong, *J. Zhejiang Univ., Sci., B*, 2008, **9**, 506–510.
- 134 G. Singh and R. S. Pai, *Drug Delivery*, 2016, **23**, 532–539.
- 135 J. Duan, J. P. Freeling, J. Koehn, C. Shu and R. J. Y. Ho, *J. Pharm. Sci.*, 2014, **103**, 2520–2529.
- 136 A. S. Nowacek, J. McMillan, R. Miller, A. Anderson, B. Rabinow and H. E. Gendelman, *J. Neuroimmune Pharmacol.*, 2010, **5**, 592–601.
- 137 M. Garg and N. K. Jain, *J. Drug Targeting*, 2006, **14**, 1–11.



- 138 H. Elkateb, L. M. Tatham, H. Cauldbeck, E. Niezabitowska, A. Owen, S. Rannard and T. McDonald, *Int. J. Pharm.*, 2020, **588**, 119794.
- 139 K. Priya Dharshini, H. Fang, D. Ramya Devi, J. X. Yang, R. H. Luo, Y. T. Zheng, M. Brzeziński and B. N. Vedha Hari, *Carbohydr. Polym.*, 2021, **256**, 117440.
- 140 A. V. Belgamwar, S. A. Khan and P. G. Yeole, *J. Drug Delivery Sci. Technol.*, 2019, **52**, 1008–1020.
- 141 R. Rozana, Y. Yulizar, A. Saefumillah and D. O. B. Apriandanu, *AIP Conf. Proc.*, 2020, **2242**, 040004.
- 142 V. Makwana, R. Jain, K. Patel, M. Nivsarkar and A. Joshi, *Int. J. Pharm.*, 2015, **495**, 439–446.
- 143 P. K. Gaur, S. Mishra, M. Bajpai and A. Mishra, *BioMed Res. Int.*, 2014, **2014**, 363404.
- 144 L. Tshweu, L. Katata, L. Kalombo, D. A. Chiappetta, C. Hocht, A. Sosnik and H. Swai, *Nanomedicine*, 2014, **9**, 1821–1833.
- 145 S. Kotta, A. W. Khan, S. H. Ansari, R. K. Sharma and J. Ali, *Int. J. Pharm.*, 2014, **462**, 129–134.
- 146 A. Shibata, E. McMullen, A. Pham, M. Belshan, B. Sanford, Y. Zhou, M. Goede, A. A. Date and C. J. Destache, *AIDS Res. Hum. Retroviruses*, 2013, **29**, 746–754.
- 147 M. de Sousa and F. B. T. Pessine, *Adv. Sci., Eng. Med.*, 2014, **6**, 1135–1142.
- 148 Y. Gong, K. Zhi, P. K. B. Nagesh, N. Sinha, P. Chowdhury, H. Chen, S. Gorantla, M. M. Yallapu and S. Kumar, *Viruses*, 2020, **12**, 564.
- 149 Y. Gong, P. Chowdhury, N. M. Midde, M. A. Rahman, M. M. Yallapu and S. Kumar, *Biochem. Biophys. Rep.*, 2017, **12**, 214–219.
- 150 T. N. Figueira, M. M. Domingues, F. Illien, I. Cadima-Couto, T. Todorovski, D. Andreu, S. Sagan, M. A. R. B. Castanho, A. Walrant and A. S. Veiga, *ACS Infectious Diseases*, 2020, **6**, 224–236.
- 151 E. Russo, N. Gaglianone, S. Baldassari, B. Parodi, S. Cafaggi, C. Zibana, M. Donalizio, V. Cagno, D. Lembo and G. Caviglioli, *Colloids Surf., B*, 2014, **118**, 117–125.
- 152 K. M. Tyo, A. B. Lasnik, L. Zhang, M. Mahmoud, A. B. Jenson, J. L. Fuqua, K. E. Palmer and J. M. Steinbach-Rankins, *J. Controlled Release*, 2020, **321**, 84–99.
- 153 Z. Karami, M. R. Saghatchi Zanjani, S. Rezaee, K. Rostamizadeh and M. Hamidi, *Drug Dev. Ind. Pharm.*, 2019, **45**, 736–744.
- 154 B. Surnar, M. Z. Kamran, A. S. Shah, U. Basu, N. Kolishetti, S. Deo, D. T. Jayaweera, S. Daunert and S. Dhar, *ACS Nano*, 2019, **13**, 11034–11048.
- 155 G. Joshi, A. Kumar and K. Sawant, *Drug Delivery*, 2016, **23**, 3492–3504.
- 156 P. R. Ravi, R. Vats, V. Dalal, N. Gadekar and N. Aditya, *Drug Dev. Ind. Pharm.*, 2015, **41**, 131–140.
- 157 A. Alex, W. Paul, A. J. Chacko and C. P. Sharma, *Ther. Delivery*, 2011, **2**, 25–35.
- 158 S. Perazzolo, L. M. Shireman, J. Koehn, L. A. McConnachie, J. C. Kraft, D. D. Shen and R. J. Y. Ho, *J. Pharm. Sci.*, 2018, **107**, 3153–3162.
- 159 L. Fotooh Abadi, P. Kumar, V. Gajbhiye, K. M. Paknikar and S. Kulkarni, *Colloids Surf., B*, 2020, **194**, 111227.
- 160 S. Lahkar and M. K. Das, *J. Nanopart. Res.*, 2020, **22**, 109.
- 161 J. Varshosaz, S. Taymouri, E. Jafari, A. Jahanian-Najafabadi and A. Taheri, *J. Drug Delivery Sci. Technol.*, 2018, **48**, 9–20.
- 162 L. N. Ramana, S. Sethuraman, U. Ranga and U. M. Krishnan, *J. Biomed. Sci.*, 2010, **17**, 1–9.
- 163 A. A. Date, A. Shibata, M. Goede, B. Sanford, K. La Bruzzo, M. Belshan and C. J. Destache, *Antiviral Res.*, 2012, **96**, 430–436.
- 164 F. Javan, A. Vatanara, K. Azadmanesh, M. Nabi-Meibodi and M. Shakouri, *J. Pharm. Pharmacol.*, 2017, **69**, 1002–1009.
- 165 S. Kumar, R. Narayan, V. Ahammed, Y. Nayak, A. Naha and U. Y. Nayak, *J. Drug Delivery Sci. Technol.*, 2018, **44**, 181–189.
- 166 I. F. Abou-El-Naga, E. D. El Kerdany, R. F. Mady, T. I. Shalaby and E. M. Zaytoun, *Parasitol. Int.*, 2017, **66**, 735–747.
- 167 S. Jain, J. M. Sharma, A. K. Jain and R. R. Mahajan, *Nanomedicine*, 2013, **8**, 1639–1655.
- 168 L. M. Bimbo, O. V. Denisova, E. Mäkilä, M. Kaasalainen, J. K. De Brabander, J. Hirvonen, J. Salonen, L. Kakkola, D. Kainov and H. A. Santos, *ACS Nano*, 2013, **7**, 6884–6893.
- 169 L. N. Ramana, S. Sharma, S. Sethuraman, U. Ranga and U. M. Krishnan, *Biochim. Biophys. Acta, Gen. Subj.*, 2014, **1840**, 476–484.
- 170 Y. C. Kuo and H. F. Ko, *Biomaterials*, 2013, **34**, 4818–4830.
- 171 J. Adlin Jino Nesalin and A. Anton Smith, *J. Pharm. Res.*, 2013, **6**, 268–274.
- 172 R. Shegokar and K. K. Singh, *Pharmazie*, 2011, **66**, 264–271.
- 173 M. Garg, A. Asthana, H. B. Agashe, G. P. Agrawal and N. K. Jain, *J. Pharm. Pharmacol.*, 2010, **58**, 605–616.
- 174 Y. C. Kuo and C. Y. Chung, *Colloids Surf., B*, 2011, **88**, 682–690.
- 175 T. Chaowanachan, E. Krogstad, C. Ball and K. A. Woodrow, *PLoS One*, 2013, **8**, 61416.
- 176 S. Mandal, P. K. Prathipati, G. Kang, Y. Zhou, Z. Yuan, W. Fan, Q. Li and C. J. Destache, *Aids*, 2017, **31**, 469–476.
- 177 S. Mandal, G. Kang, P. K. Prathipati, Y. Zhou, W. Fan, Q. Li and C. J. Destache, *J. Controlled Release*, 2019, **294**, 216–225.
- 178 J. Shailender, P. R. Ravi, M. Reddy Sirukuri, A. Dalvi and O. Keerthi Priya, *Drug Dev. Ind. Pharm.*, 2018, **44**, 1109–1119.
- 179 B. Gourdon, C. Chemin, A. Moreau, T. Arnauld, P. Baumy, S. Cisternino, J. M. Péan and X. Declèves, *Int. J. Pharm.*, 2017, **529**, 357–370.
- 180 R. Kumar and V. R. Sinha, *AAPS PharmSciTech*, 2017, **18**, 884–894.
- 181 S. M. T. Cavalcanti, C. Nunes, S. A. Costa Lima, J. L. Soares-Sobrinho and S. Reis, *Eur. J. Pharm. Sci.*, 2018, **122**, 22–30.
- 182 J. K. Yan, Y. Y. Wang, W. Y. Qiu and J. Y. Wu, *Carbohydr. Polym.*, 2017, **174**, 209–216.
- 183 M. Da Silva Barbi, F. C. Carvalho, C. P. Kiill, H. Da Silva Barud, S. H. Santagneli, S. J. L. Ribeiro and M. P. D. Gremião, *J. Nanosci. Nanotechnol.*, 2015, **15**, 865–874.





Review

- 184 D. D. Kumbhar and V. B. Pokharkar, *Colloids Surf., A*, 2013, **436**, 714–725.
- 185 R. M. Mainardes, N. M. Khalil and M. P. D. Gremião, *Int. J. Pharm.*, 2010, **395**, 266–271.
- 186 S. Singh, A. K. Dobhal, A. Jain, J. K. Pandit and S. Chakraborty, *Chem. Pharm. Bull.*, 2010, **58**, 650–655.
- 187 P. Kumar, Y. S. Lakshmi and A. K. Kondapi, *Pharm. Res.*, 2017, **34**, 257–268.

